

# How perturbative are heavy sea quarks?



Andreas Athenodorou<sup>a,b</sup>, Jacob Finkenrath<sup>b</sup>, Francesco Knechtli<sup>c</sup>, Tomasz Korzec<sup>c</sup>,  
Björn Leder<sup>d</sup>, Marina Krstić Marinković<sup>e</sup>, Rainer Sommer<sup>f,d</sup>

<sup>a</sup> Department of Physics, University of Cyprus, P.O. Box 20537, Nicosia CY, Cyprus

<sup>b</sup> CaSToRC, CyI Athalassa Campus, 20 Constantinou Kavafi Street, 2121 Nicosia, Cyprus

<sup>c</sup> Department of Physics, Bergische Universität Wuppertal, Gaussstr. 20, 42119 Wuppertal, Germany

<sup>d</sup> Institut für Physik, Humboldt-Universität zu Berlin, Newtonstr. 15, 12489 Berlin, Germany

<sup>e</sup> School of Mathematics, Trinity College, Dublin 2, Ireland

<sup>f</sup> John von Neumann Institute for Computing (NIC), DESY, Platanenallee 6, D-15738 Zeuthen, Germany

## Abstract

Effects of heavy sea quarks on the low energy physics are described by an effective theory where the expansion parameter is the inverse quark mass,  $1/M$ . At leading order in  $1/M$  (and neglecting light quark masses) the dependence of any low energy quantity on the heavy quark mass is given in terms of the ratio of  $\Lambda$  parameters of the effective and the fundamental theory. We define a function describing the scaling with the mass  $M$ . Our study of perturbation theory suggests that its perturbative expansion is very reliable for the bottom quark and also seems to work very well at the charm quark mass. The same is then true for the ratios of  $\Lambda^{(4)}/\Lambda^{(5)}$  and  $\Lambda^{(3)}/\Lambda^{(4)}$ , which play a major rôle in connecting (almost all) lattice determinations of  $\alpha_{\overline{\text{MS}}}^{(3)}$  from the three-flavor theory with  $\alpha_{\overline{\text{MS}}}^{(5)}(M_Z)$ . Also the charm quark content of the nucleon, relevant for dark matter searches, can be computed accurately from perturbation theory.

In order to further test perturbation theory in this situation, we investigate a very closely related model, namely QCD with  $N_f = 2$  heavy quarks. Our non-perturbative information is derived from simulations on the lattice, with masses up to the charm quark mass and lattice spacings down to about 0.023 fm followed by a continuum extrapolation. The non-perturbative mass dependence agrees within rather small errors with the perturbative prediction at masses around the charm quark mass. Surprisingly, from studying solely the massive theory we can make a prediction for the ratio  $Q_{0,2}^{\sqrt{t_0}} = [\Lambda\sqrt{t_0(0)}]_{N_f=2}/[\Lambda\sqrt{t_0}]_{N_f=0}$ , which refers to the chiral limit in  $N_f = 2$ . Here  $t_0$  is the Gradient Flow scale of [1]. The uncertainty for  $Q$  is estimated to be dominated by the statistical errors of below 2%. For the phenomenologically interesting  $\Lambda^{(3)}/\Lambda^{(4)}$ , we conclude that perturbation theory introduces errors which are at most at the 0.5% level, far smaller than other current uncertainties.

**Keywords:** Lattice QCD, Decoupling, Effective theory, Matching of Lambda parameters, Charm quark, Dark matter

**PACS:** 12.38.Gc, 12.38.Bx, 14.65.Dw

## Contents

<b>1</b>	<b>Introduction</b>	<b>2</b>
<b>2</b>	<b>The effective theory: decQCD</b>	<b>3</b>
<b>3</b>	<b>Mass-dependence in the leading order effective theory</b>	<b>5</b>
3.1	Non-perturbative matching and mass-dependence . . . . .	6
3.2	Perturbation theory . . . . .	7
3.2.1	Matching of couplings . . . . .	7
3.2.2	Mass scaling function $\eta^M$ . . . . .	8
3.3	Accuracy of perturbation theory . . . . .	9
<b>4</b>	<b>Non-perturbative investigation for <math>N_f = 2 \rightarrow N_l = 0</math></b>	<b>13</b>
4.1	Low energy observables . . . . .	14
4.2	Fixing the RGI parameters of the theory and details of the simulations . . .	14
4.2.1	Discretization . . . . .	14
4.2.2	$O(a)$ improvement and finite size effects . . . . .	15
4.2.3	Quark masses . . . . .	15
4.2.4	Hadronic scales on the lattice . . . . .	16
4.2.5	Simulation algorithms . . . . .	17
4.2.6	Autocorrelation times and error analysis . . . . .	18
<b>5</b>	<b>Non-perturbative mass dependence</b>	<b>19</b>
5.1	Test of the factorization formula . . . . .	19
5.2	The mass-scaling function $\eta^M$ . . . . .	21
<b>6</b>	<b>How big are the effects of charm loops?</b>	<b>24</b>
6.1	Heavy quark content of the nucleon . . . . .	25
6.2	From the model to QCD . . . . .	26
<b>7</b>	<b>Conclusions</b>	<b>26</b>
<b>A</b>	<b>Expansion of the matching condition and the mass scaling function</b>	<b>27</b>
<b>B</b>	<b>Asymptotic expression for <math>P(M/\Lambda)</math></b>	<b>28</b>
<b>C</b>	<b>Simulation parameters</b>	<b>29</b>
C.1	Mass corrections . . . . .	29

## 1 Introduction

At present most simulations of lattice Quantum Chromodynamics (QCD) include two light (up and down) quarks and a strange quark. It is important to investigate the effects of the charm quark, whose mass  $M$  is about 12 times larger than that of the strange quark. Effective field theory [2] arguments predict that the effects of a heavy quark are described by the theory without the heavy quark with leading order power corrections of size  $O(1/M^2)$ . At lowest order in  $1/M$  only the light quark masses and the coupling need to be adjusted

to match the two theories (with and without the heavy quarks). For the coupling this issue has been discussed in perturbation theory in [3]. The matching of the coupling in the case of the decoupling of one heavy quark is known to four loops in perturbation theory [4, 5]. Equivalently to match the couplings at a given renormalization scale one can formulate a relation between the renormalization group invariant  $\Lambda$  parameters of the effective and the fundamental theory. In this article we present a study of the perturbative behaviour of the ratio of  $\Lambda$  parameters computed up to four loops in the matching of the couplings, which requires the knowledge of the five loop  $\beta$  function, which had been computed in Refs. [6–10].

Besides studying the behaviour of perturbation theory itself it is desirable to compare to non-perturbative data. This is especially the case for the charm quark given that matching is performed at a fairly low scale  $\approx 1.3 \text{ GeV}$  in this case. It is very difficult to compare directly 2+1 flavor and 2+1+1 flavor lattice simulations, because various systematic uncertainties mask the physical effect. We proposed instead to simulate a model, namely QCD with two heavy, mass-degenerate quarks [11]. The effective theory is the Yang-Mills theory up to  $1/M^2$  corrections. The mass dependence of ratios of hadronic scales such as  $K^{\text{had}}(M) = \sqrt{t_0(0)}/\sqrt{t_0(M)}$ , where  $t_0$  is the Gradient flow scale [1] factorizes [11] at leading order in a non-perturbative and mass-independent factor, and a factor  $P$ , which is the ratio of the  $\Lambda$  parameters and depends on the heavy quark mass through the matching. Since the latter can be evaluated in perturbation theory we can compare the perturbative mass dependence of hadronic scales to the non-perturbative results from the simulations. We define a mass-scaling function which is the logarithmic derivative of  $P$  with respect to the logarithm of the mass. It can be determined directly from the simulations and compared to its perturbative expansion.

This article is organized as follows. In section 2 we describe the effective theory of decoupling. Section 3 contains a review of the matching of the effective and fundamental theory at leading order. We present a perturbative study of the ratio  $P$  of the  $\Lambda$  parameters, which results from the matching of the theories at leading order, and of the mass-scaling function. In section 4 we explain our non-perturbative study of decoupling in a theory with  $N_f = 2$  mass-degenerate heavy fermions with masses ranging up to (slightly above) the charm quark mass. We introduce the hadronic scales which we calculate in Monte Carlo simulations of lattice QCD and give details of the lattice simulations. The comparison of the non-perturbative mass dependence of hadronic scales computed from the simulations with perturbation theory is presented in section 5. The implications of these results for the applicability of perturbation theory at the scale of the charm quark mass are discussed in section 6. We summarize our results in section 7. In the appendix A we reproduce the explicit formulae for the matching of the couplings up to four loops and the perturbative coefficients of the mass-scaling function. The asymptotic behavior for large masses of  $P$  is derived in appendix B. Finally appendix C contains tables listing the simulations parameters.

## 2 The effective theory: decQCD

The effective theory associated with the decoupling of heavy quarks is formally obtained by integrating out the heavy quark fields. The resulting effective theory contains a tower of non-renormalizable interactions, which however are suppressed at low energies by negative

powers of the heavy quark masses [2]. The (infinite number of) couplings of the effective theory can be matched order by order and used to describe the effect of heavy quarks at low energies.

To be precise, let us consider  $\text{QCD}_{N_f}$  with  $N_f$  quarks in total, of which  $N_l$  are light and  $N_f - N_l$  are heavy. For simplicity we assume the light and the heavy quarks to be mass degenerate with the heavy mass given by  $M$ . Non-degenerate quark masses are conceptually similar, see note at the end of this section. In general the Lagrangian of the effective theory is

$$\mathcal{L}_{\text{dec}} = \mathcal{L}_0 + \frac{1}{M}\mathcal{L}_1 + \frac{1}{M^2}\mathcal{L}_2 + \dots, \quad (2.1)$$

where the leading order equals  $\text{QCD}_{N_l}$  with  $N_l$  quarks and the corrections  $\mathcal{L}_k$ ,  $k \geq 1$  consist of linear combinations of local operators of dimension  $4+k$ . These operators are composed of only the light quark and gauge fields, and include possible light mass factors. They have to satisfy the symmetries of  $\text{QCD}_{N_f}$ , most prominently gauge, Euclidean (or Lorentz) and chiral invariance. For the cases of interest, operators of dimension five are excluded and corrections to the leading order start at  $\mathcal{O}(M^{-2})$

$$\mathcal{L}_{\text{dec}} = \mathcal{L}_{\text{QCD}_{N_l}} + \frac{1}{M^2} \sum_i \omega_i \Phi_i + \dots. \quad (2.2)$$

Here we write  $\mathcal{L}_2$  explicitly as a linear combination of local dimension six operators  $\Phi_i$ , multiplied by dimensionless couplings  $\omega_i$ .

The simplest situation in which (2.2) holds is  $N_l = 0$ , i.e., when light quarks are absent: the leading order is Yang-Mills theory and there is no gauge invariant dimension five operator made up of gauge fields alone. Thus at leading order only the gauge coupling has to be matched. We are basing our non-perturbative investigations in sections 4-5 on this setting.

In the presence of  $N_l \geq 2$  mass-less quarks the non-singlet, non-anomalous chiral symmetry in the light quark sector forbids any dimension five operator. The gauge coupling is still the only coupling to be matched at leading order. Note that the dynamical (non-perturbative) breaking of chiral symmetry plays no role here as we may consider full and effective theory in a finite (but large) volume where dynamical symmetry breaking is absent, in full analogy with the elegant derivation of automatic  $\mathcal{O}(a)$  improvement of twisted mass QCD in [12]. More explicitly consider a chirally non-invariant observable in the full theory in finite volume. It vanishes, while a priori in the effective theory at dimension five the Pauli term  $\omega_{\text{Pauli}} \bar{\psi} i \sigma_{\mu\nu} F_{\mu\nu} \psi / M$  contributes as the only dimension five gauge invariant operator. Matching of full and effective theory requires  $\omega_{\text{Pauli}} = 0$ .

In section 3 we consider the leading order in  $1/M$  in perturbation theory for various values of  $N_l, N_f$ .

For finite light quark masses there are dimension five operators, which are formed of the operators in  $\mathcal{L}_{\text{QCD}_{N_l}}$  multiplied by the light quark masses. Their effect can be absorbed in a redefinition of the gauge coupling and light quark masses at the order  $m_l/M$ . The Pauli term multiplied by the light quark masses contributes at dimension six. It is one of the  $\Phi_i$  in eq. (2.2). Besides the gauge coupling now also the light quark mass needs to be matched.

All in all, finite light quark masses do not change the structure of eq. (2.2). Of course couplings in the effective Lagrangian now also depend on the light quark mass. The only restriction is that when light quarks are present, we need at least a doublet, such that there is a non-anomalous chiral symmetry of the mass-less theory and we can conclude  $\omega_{\text{Pauli}} = 0$  as sketched above.

In the following we concentrate on  $N_l \geq 2$  mass-less or  $N_l = 0$  quarks.

### 3 Mass-dependence in the leading order effective theory

At leading order, the only parameter of the effective theory,  $\text{QCD}_{N_l}$ , is its running coupling and the theory predicts all observables when the coupling is prescribed at a given renormalization scale in a given renormalization scheme. It is conceptually cleaner, but completely equivalent in terms of the physical content to specify the renormalization group invariant (RGI)  $\Lambda$ -parameter. The scale dependence of the input is then gone and the scheme-dependence is easily computable: the one-loop relation of couplings yields the exact relation of the associated  $\Lambda$ -parameters.

Explicitly the  $\Lambda$ -parameter of QCD with  $N_f$  quarks

$$\Lambda_f = \mu (b_0 \bar{g}^2)^{-b_1/(2b_0^2)} e^{-1/(2b_0 \bar{g}^2)} \exp \left\{ - \int_0^{\bar{g}} dx \left[ \frac{1}{\beta_f(x)} + \frac{1}{b_0 x^3} - \frac{b_1}{b_0^2 x} \right] \right\} \quad (3.1)$$

is defined as the integration constant of the solution to the renormalization group equation (RGE) for the renormalised coupling

$$\mu \frac{\partial \bar{g}}{\partial \mu} = \beta_f(\bar{g}) \quad (3.2)$$

with the QCD  $\beta$ -function

$$\begin{aligned} \beta_f(\bar{g}) &\stackrel{\bar{g} \rightarrow 0}{\sim} -\bar{g}^3 \{b_0 + \bar{g}^2 b_1 + \dots\} , \\ b_0 &= \frac{1}{(4\pi)^2} \left( 11 - \frac{2}{3} N_f \right) , \quad b_1 = \frac{1}{(4\pi)^4} \left( 102 - \frac{38}{3} N_f \right) . \end{aligned} \quad (3.3)$$

We shall also make use of the RGI mass  $M$

$$M = \bar{m} (2b_0 \bar{g}^2)^{-d_0/(2b_0)} \exp \left\{ - \int_0^{\bar{g}} dx \left[ \frac{\tau_f(x)}{\beta_f(x)} - \frac{d_0}{b_0 x} \right] \right\} \quad (3.4)$$

which appears as an integration constant in the solution of the RGE for the renormalised mass

$$\frac{\mu}{\bar{m}} \frac{\partial \bar{m}}{\partial \mu} = \tau_f(\bar{g}) , \quad (3.5)$$

$$\tau_f(\bar{g}) \stackrel{\bar{g} \rightarrow 0}{\sim} -\bar{g}^2 \{d_0 + \bar{g}^2 d_1 + \dots\} , \quad d_0 = 8/(4\pi)^2 . \quad (3.6)$$

In the following subsection we discuss how the relation of the  $\Lambda$ -parameters of fundamental and effective theory determine the (heavy-) mass dependence of low energy observables and then turn to the available perturbative information.

### 3.1 Non-perturbative matching and mass-dependence

The leading order (in  $1/M$ ) effective theory describes the fundamental one at low energy when  $\Lambda_l$  has the proper value. In other words, it has to be chosen as a function  $\Lambda_{\text{dec}}$  of  $M$  and  $\Lambda_f$ ,

$$\Lambda_l = \Lambda_{\text{dec}}(M, \Lambda_f). \quad (3.7)$$

Of course this information is equivalent to the matching relation of the couplings. It is natural to introduce the equivalent dimensionless function  $P_{l,f}$  via

$$\Lambda_{\text{dec}}(M, \Lambda_f) = P_{l,f}(M/\Lambda_f) \Lambda_f. \quad (3.8)$$

One may ask the question, in how far  $P_{l,f}$  is unique. As long as  $M$  is large enough such that one can neglect order  $1/M^2$  terms it is unique and in perturbation theory such terms can always be neglected. Beyond perturbation theory, a precise definition of  $P_{l,f}$  also requires to specify one quantity that is matched between effective and fundamental theory. Denoting it by  $\mathcal{Q}$ , the statement of uniqueness then means

$$P_{l,f}^{\mathcal{Q}1}(M/\Lambda_f) = P_{l,f}^{\mathcal{Q}2}(M/\Lambda_f) + \mathcal{O}((\Lambda_f/M)^2), \quad (3.9)$$

in obvious notation. We will drop the dependence on  $\mathcal{Q}$  from now on, and note that the subsequent statements all have the  $\mathcal{O}((\Lambda_f/M)^2)$  fuzziness, even when we do not indicate it explicitly.

Once the theories are matched, i.e. eq. (3.8) is used, hadron masses are equal in the two theories,

$$m_f^{\text{had}} = m_l^{\text{had}} + \mathcal{O}((\Lambda_f/M)^2). \quad (3.10)$$

In the low energy theory  $\text{QCD}_{N_l}$  there are no mass parameters. Thus

$$\rho^{\text{had}} = m_l^{\text{had}}/\Lambda_l \quad (3.11)$$

are pure numbers, independent of  $M$ . In the fundamental theory  $m_f^{\text{had}}(M)/\Lambda_f$  depends on  $M$ , but only through  $m_f^{\text{had}}(M)$ . The RGI  $\Lambda_f$  does not depend on  $M$  by definition. For the mass dependence of  $m_f^{\text{had}}$  we therefore obtain

$$K^{\text{had}}(M) \equiv \frac{m_f^{\text{had}}(M)}{m_f^{\text{had}}(0)} = Q_{l,f}^{\text{had}} \times P_{l,f}(M/\Lambda_f) \quad (3.12)$$

with

$$Q_{l,f}^{\text{had}} = \frac{m_l^{\text{had}}/\Lambda_l}{m_f^{\text{had}}(0)/\Lambda_f} \quad (3.13)$$

defined entirely through the two mass-less theories. We call eq. (3.12) *factorisation formula* because it separates the mass dependence into a “perturbative” (see section 3.2) factor  $P_{l,f}$  and a non-perturbative factor  $Q_{l,f}^{\text{had}}$  respectively. In the same loose sense as usually used in factorisation formulae, the long-distance physics is in  $Q$  while the short-distance one is in  $P$ . The scale for long/short is given by  $1/M$ . We have “perturbative” in quotes, because

the meaning is not that perturbation theory gives the complete answer but that it yields an asymptotic expansion.

In all the above, we may replace hadron masses by the inverse of hadronic low energy length scales such as  $r_0$ ,  $\sqrt{t_0}$ ,  $w_0$  [1, 13, 14] which are often used for scale setting [15] or to investigate the dependence of QCD on the number of flavors [16]. We will explain them in more detail in section 4.1.

To simplify the notation, we will from now on omit the subscripts l, f when referring to the quantities  $Q$ ,  $P$ .

An interesting consequence of these considerations ((3.8) and (3.12)) is that the mass-scaling function ( $P'(x) = \frac{d}{dx}P(x)$ )

$$\eta^M(M) \equiv \frac{M}{P} \frac{\partial P}{\partial M} \Big|_{\Lambda_f} = \frac{M}{\Lambda_f} \frac{P'}{P} \quad (3.14)$$

can be computed in perturbation theory when  $M$  is sufficiently large, cf. [17]. A completely non-perturbative information only remains in the factor  $Q$  in eq. (3.12).

We can estimate  $\eta^M$  from the mass dependence of hadronic quantities by taking the logarithmic derivative in eq. (3.12) with respect to the logarithm of the mass

$$\frac{M}{m_f^{\text{had}}(M)} \frac{\partial m_f^{\text{had}}(M)}{\partial M} \Big|_{\Lambda_f} = \eta^M, \quad (3.15)$$

where  $m_f^{\text{had}}(0)$  drops out. Of course the  $\Lambda^2/M^2$  dependence on  $\mathcal{Q}$  in eq. (3.9) are inherited by  $\eta^M$ .

## 3.2 Perturbation theory

### 3.2.1 Matching of couplings

We consider a mass-independent renormalization scheme; whenever we insert perturbative coefficients, it will be in the  $\overline{\text{MS}}$ -scheme.

Since the heavy quarks contribute through loops, there is a relation between the  $\overline{\text{MS}}$ -couplings  $\bar{g}_f(\mu/\Lambda_f)$  of the fundamental theory and  $\bar{g}_{\text{dec}}(\mu/\Lambda_{\text{dec}})$  of the leading order effective theory. To simplify the notation we use  $\bar{g}(\mu/\Lambda) \equiv \bar{g}_f(\mu/\Lambda_f)$ . The relation is

$$\bar{g}_{\text{dec}}^2(\mu/\Lambda_{\text{dec}}) = \bar{g}^2(\mu/\Lambda) + \mathcal{O}(\bar{g}^4(\mu/\Lambda)). \quad (3.16)$$

In perturbation theory, power corrections can be separated from the logarithmic  $\bar{g}^2$  terms and the relation is universal, i.e. independent of the matching condition. Choosing the particular scale  $\mu = m_*$  [2, 3], the first correction vanishes and we have [4, 18]

$$\bar{g}_{\text{dec}}^2(m_*/\Lambda_{\text{dec}}) = \bar{g}^2(m_*/\Lambda) C(\bar{g}(m_*/\Lambda)) \quad (3.17)$$

$$C(g) = 1 + c_2 g^4 + c_3 g^6 + c_4 g^8 + \dots \quad (3.18)$$

The scale  $m_*$  is defined such that the renormalised quark mass fulfills  $\bar{m}(m_*) = m_*$ . The two loop coefficient is then given by  $c_2 = (N_f - N_l) \frac{11}{72} (4\pi^2)^{-2}$ . The coefficients  $c_3$  and  $c_4$  are known for  $N_f - N_l = 1, 2$  and  $N_f - N_l = 1$ , respectively. They are listed in Appendix A.

### 3.2.2 Mass scaling function $\eta^M$

In order to find the perturbative expansion of  $\eta^M$ , eq. (3.14), we start from the related function

$$\eta^m = \frac{m_*}{P} \left. \frac{\partial P}{\partial m_*} \right|_{\Lambda}, \quad (3.19)$$

which appears upon taking a derivative with respect to the logarithm of  $m_*$  on both sides of eq. (3.17). The left hand side yields

$$m_* \frac{\partial \bar{g}_{\text{dec}}^2(m_*/\Lambda_{\text{dec}})}{\partial m_*} = 2\bar{g}_1\beta_1(\bar{g}_1) [1 + \eta^m], \quad (3.20)$$

where we used the matching condition  $\bar{g}_{\text{dec}}(m_*/\Lambda_{\text{dec}}) = \bar{g}_1(m_*/(P\Lambda))$ . Combined with the straightforward derivative of the right hand side we can solve for  $\eta^m$  and obtain

$$\eta^m = 1 - \frac{\beta_f(\bar{g})}{\beta_1(\bar{g})\tilde{C}(\bar{g})} \left[ \tilde{C}(\bar{g}) + \bar{g} \frac{d}{d\bar{g}} \tilde{C}(\bar{g}) \right], \quad \tilde{C}(g) = \sqrt{C(g)}, \quad (3.21)$$

where we used eq. (3.17) to replace  $\bar{g}_1 = \bar{g}\tilde{C}(\bar{g})$ . Finally, with  $\frac{M}{m_*} \frac{\partial m_*}{\partial M} = (1 - \tau_f)^{-1}$ , (see eg. [19], section 3.3.2) we derive

$$\eta^M = \frac{\eta^m}{1 - \tau_f}. \quad (3.22)$$

The first terms in the perturbative expression

$$\eta^m = \eta_0 + \eta_1 \bar{g}^2 + \eta_2 \bar{g}^4 + \eta_3 \bar{g}^6 + \eta_4 \bar{g}^8 + \dots \quad (3.23)$$

are given by

$$\eta_0 = 1 - \frac{b_0(N_f)}{b_0(N_1)} > 0, \quad \eta_1 = (\eta_0 - 1) \left[ \tilde{b}_1(N_f) - \tilde{b}_1(N_1) \right], \quad (3.24)$$

with  $\tilde{b}_i(N_f) = b_i(N_f)/b_0(N_f)$ . The flavor dependence of the coefficients of the QCD  $\beta$ -function (3.3) is made explicit here. The perturbative expansion of  $\eta^M$

$$\eta^M = \eta_0 + \eta_1^M \bar{g}^2 + \eta_2^M \bar{g}^4 + \eta_3^M \bar{g}^6 + \eta_4^M \bar{g}^8 + \dots, \quad (3.25)$$

is obtained from (3.22) and the coefficients are given by the recursion

$$\eta_i^M = \eta_i - \sum_{j=0}^{i-1} d_j \eta_{i-1-j}^M. \quad (3.26)$$

For example  $\eta_1^M = \eta_1 - d_0 \eta_0$ , where  $d_0$  is the universal coefficient of the QCD anomalous dimension (3.6). The higher order coefficients  $\eta_i$ , up to  $i = 4$ , are collected in appendix A.

We note that for fixed  $N_1$  the first two coefficients are exactly proportional to  $N_f - N_1$

$$\eta_0 = \frac{2(N_f - N_1)}{33 - 2N_1}, \quad \eta_1 = \frac{642(N_f - N_1)}{(4\pi)^2(33 - 2N_1)^2}, \quad \eta_1^M = \frac{2(57 + 16N_1)(N_f - N_1)}{(4\pi)^2(33 - 2N_1)^2}. \quad (3.27)$$



$N_f$	$N_l$	$\eta_0$	$\eta_1$	$\eta_1^M$	$\eta_1^M/2b_0(N_f)$	$\log(k)$
2	0	0.121212	0.007467	0.001326	0.010829	0.046655
5	3	0.148148	0.011154	0.003648	0.037574	0.017501
4	3	0.074074	0.005577	0.001824	0.017284	0.012756
5	4	0.080000	0.006505	0.002452	0.025252	0.002622

**Table 1:** Numerical size of the perturbative coefficients in eqs. (3.23), (3.25) and (3.28).

At higher orders this is only true up to small corrections. The dependence on  $N_l$  at fixed  $N_f - N_l$  is weak and amounts to a difference of about 20% at leading order between  $N_l = 0$  and  $N_l = 3$ . In table 1 we list numerical values for interesting combinations of  $N_f$  and  $N_l$ .

Integrating eq. (3.14) now gives an asymptotic expression for the mass dependence of non-perturbative low energy scales  $m_f^{\text{had}}$  from perturbation theory ( $\ell = \log(M/\Lambda)$ )

$$P = \frac{1}{k} \exp(\eta_0 \ell) \ell^{\eta_1^M/(2b_0(N_f))} \times \left[ 1 + \mathcal{O}\left(\frac{\log(\ell)}{\ell}\right) \right], \quad (3.28)$$

where the constant  $k$  is fixed by the standard convention for the  $\Lambda$ -parameter and the less standard convention of Gasser and Leutwyler for the RGI mass  $M$ , which we reproduce in eq. (3.4),

$$\log(k) = \frac{\tilde{b}_1(N_f)}{2b_0(N_f)} \log(2) - \frac{\tilde{b}_1(N_l)}{2b_0(N_l)} \log(2b_0(N_f)/b_0(N_l)). \quad (3.29)$$

See Appendix B for the derivation of eq. (3.28). We note that the leading correction in the expansion eq. (3.28) is  $\log(\ell)/\ell$ . It contains a term  $g_*^2 \log(g_*^2)$ , cf. eq. (B.5), which makes the convergence of the expansion slow. Therefore for the numerical evaluation of  $P$  we prefer to use the formula eq. (3.30) which has corrections only in powers of  $g_*^2$  (no logarithms), see the details in section 3.3. Accidentally, for the interesting cases, the asymptotic expression eq. (3.28) for  $P$  is dominated by  $\exp(\eta_0 \ell) = (M/\Lambda)^{\eta_0}$ . This can be seen by the numerical smallness of  $\eta_1^M/2b_0(N_f)$  and  $\log(k)$  in table 1.

### 3.3 Accuracy of perturbation theory

A consistency check on the applicability of perturbation theory is the comparison of different orders. Indeed, figures 1-3 show that higher orders do not contribute very much, in particular when one uses the mass dependence in terms of the RGI mass,  $\eta^M$ . This also suggests that it is an advantage to consider the perturbative prediction for  $P$  in terms of  $M/\Lambda$  instead of working with  $m_*/\Lambda$ . We have worked with  $M/\Lambda$  in [11] and will do so below in our comparison to a non-perturbative investigation.

Details for  $\eta^m$  and  $\eta^M$  are seen in figure 1-3. In the legends of the plots the number of loops corresponds to the highest loop order of the  $\beta$  function which is used. We note that in the right plot of figure 2 the 5-loop correction is larger in magnitude than the 4-loop correction for  $g^2 \gtrsim 3$ . But the corrections are amazingly small.

Renormalization group improved perturbative predictions for the function  $P(M/\Lambda) = \Lambda_l/\Lambda_f$  can be obtained from (cf. eq. (3.1))

$$P(M/\Lambda) = \exp \left\{ I_g^l(g_* \tilde{C}(g_*)) - I_g^f(g_*) \right\}, \quad (3.30)$$

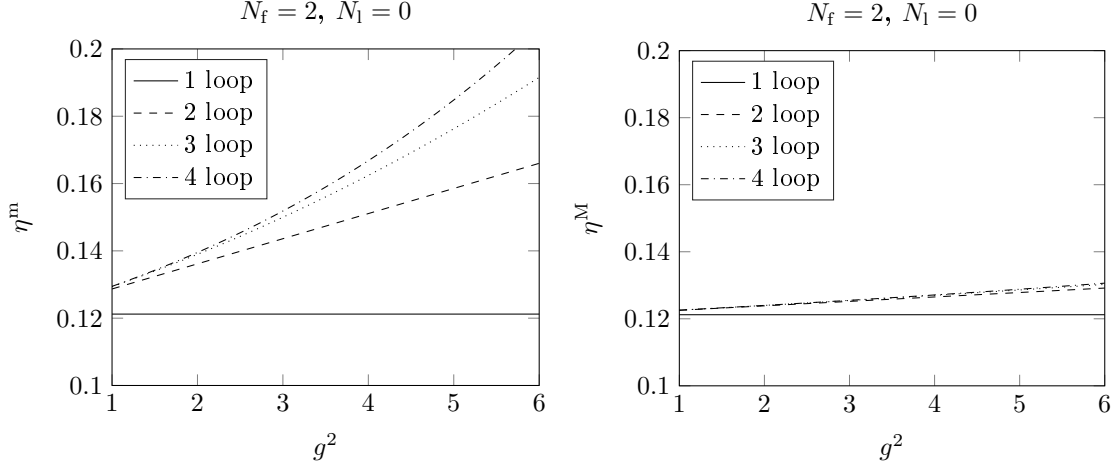


**Figure 1:** The functions  $\eta^m(g^2), \eta^M(g^2)$  for the case  $N_f = 2, N_l = 0$ . The number of loops corresponds to the highest loop order of the  $\beta$  function which is used.

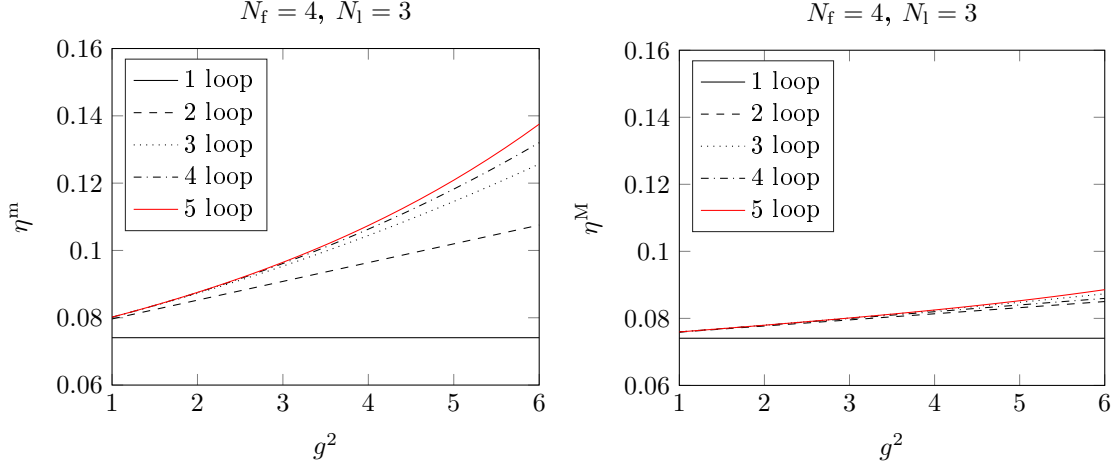


**Figure 2:** The functions  $\eta^m(g^2), \eta^M(g^2)$  for the case  $N_f = 4, N_l = 3$ . The number of loops corresponds to the highest loop order of the  $\beta$  function which is used.

where

$$\exp(I_g^i(\bar{g})) = (b_0(N_i)\bar{g}^2)^{-b_1(N_i)/(2b_0(N_i)^2)} e^{-1/(2b_0(N_i)\bar{g}^2)} \quad (3.31)$$

$$\times \exp \left\{ - \int_0^{\bar{g}} dx \left[ \frac{1}{\beta_i(x)} + \frac{1}{b_0(N_i)x^3} - \frac{b_1(N_i)}{b_0(N_i)^2 x} \right] \right\} . \quad (3.32)$$

The coupling  $g_* = \bar{g}(m_*)$  is obtained from inverting

$$\frac{\Lambda}{M} = \exp \left\{ - \int^{g_*(M/\Lambda)} dx \frac{1 - \tau_f(x)}{\beta_f(x)} \right\} , \quad (3.33)$$

where  $M$  is the RGI mass corresponding to  $m_*$ . For this equation we have combined eqs. (3.1) and (3.4) using  $\mu = \bar{m} = m_*$ . For reference the resulting relation is plotted in the left panel of figure 4 together with the values for  $M_c/\Lambda$  and  $M_b/\Lambda$  which were obtained

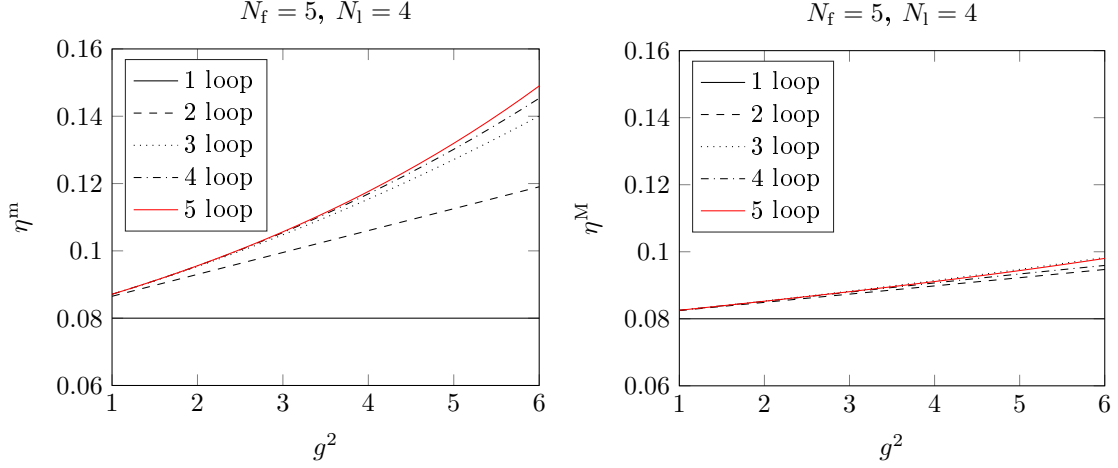


**Figure 3:** The functions  $\eta^m(g^2), \eta^M(g^2)$  for the case  $N_f = 5, N_l = 4$ . The number of loops corresponds to the highest loop order of the  $\beta$  function which is used.

from the PDG values [20] for  $\bar{m}_c/\Lambda$  and  $\bar{m}_b/\Lambda$ , and inverting eq. (3.1). Of course, in case of the charm quark  $N_f = 4$  and in the case of the bottom quark  $N_f = 5$  were used.

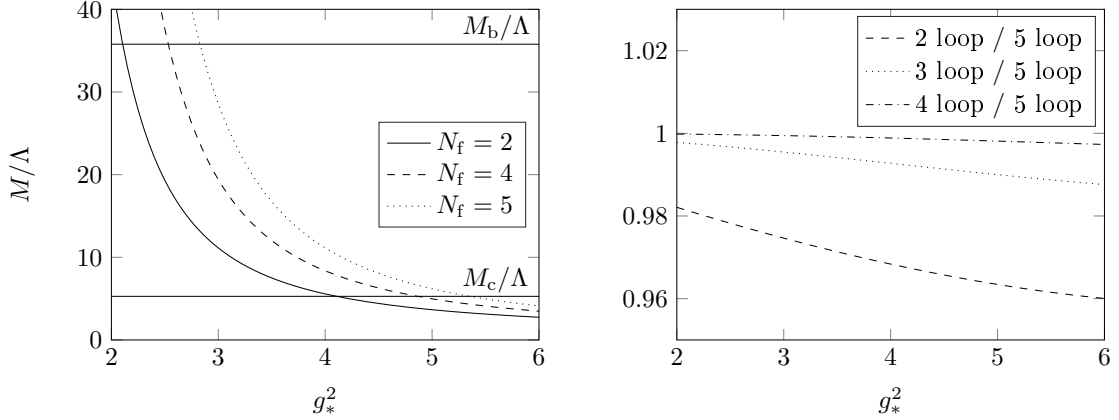


**Figure 4:** Left: The relation between  $M/\Lambda$  and  $g_*$  at 5-loop. Right: The 2, 3 and 4-loop relation divided by the 5-loop one for the case of  $N_f = 2, N_l = 0$ .

The predictions for different orders of perturbation theory are very close to the unsystematic one-loop “approximation”,  $P^{(1)} = (M/\Lambda)^{\eta_0}$ , as long as  $M/\Lambda < 30$  or so and the number of flavors is small. This is accidental. In figure 5–7 we plot the one-loop “approximation” and the 4-loop result on the left and the relative correction

$$(P - P^{(1)})/P^{(1)}. \quad (3.34)$$

at 2,3,4-loop on the right. When it is available we also add the 5-loop result. In this comparison, when we consider at least 2-loop precision, we always work to a consistent order in the renormalization group functions. Note that we do not truncate the renormalization group functions  $\beta, \tau$  in the integrals eq. (3.32), eq. (3.33), instead we expand the integrand.

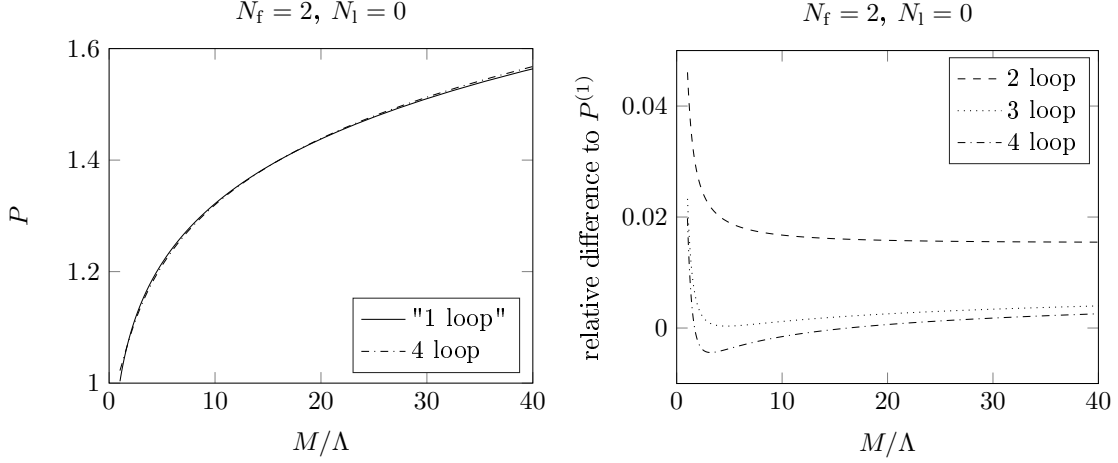


**Figure 5:** The mass-dependence  $P$  at 1-loop formula and at 4-loop (left) as well as 2,3,4-loop correction normalised to the 1-loop approximation (right) for the case  $N_f = 2, N_l = 0$ .

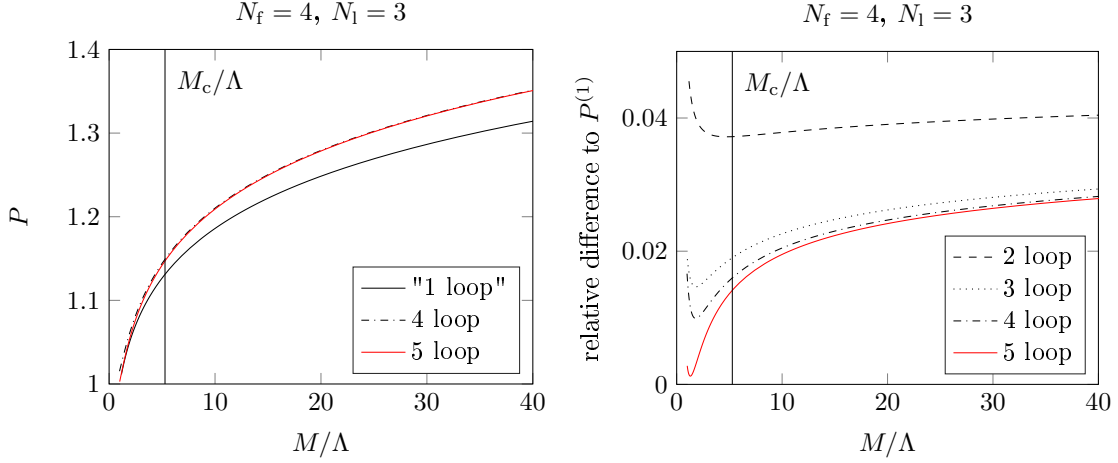


**Figure 6:** The mass-dependence  $P$  at 1-loop formula and at 4,5-loop (left) as well as 2,3,4,5-loop correction normalised to the 1-loop approximation (right) for the case  $N_f = 4, N_l = 3$ .

2-loop accuracy means dropping  $b_2, d_1$  and higher in this expansion, e.g.

$$\frac{1 - \tau(x)}{\beta(x)} = -\frac{1}{b_0 x^3} + \frac{b_1}{b_0^2 x} - \frac{d_0}{b_0 x} + \mathcal{O}(x). \quad (3.35)$$

The function  $C(g)$  only enters at 3-loop precision since  $c_1 = 0$ .

In the numerical results we observe in particular that for the phenomenologically relevant case of  $N_f = 5, N_l = 4$ , the 3-loop contribution (difference 3-loop to 2-loop) is around 2% while the 4- and 5-loop ones are then nice and small, see the right plot in figure 7. Judging by perturbation theory alone, the perturbative prediction for decoupling the b-quark should be very reliable. Also for the other phenomenologically relevant case of decoupling the c-quark ( $N_f = 4, N_l = 3$ ) perturbation theory appears to work quite well.

These curves suggest that perturbative decoupling introduces only errors at the sub-percent level for the ratios of Lambda parameters, once perturbation theory applies at

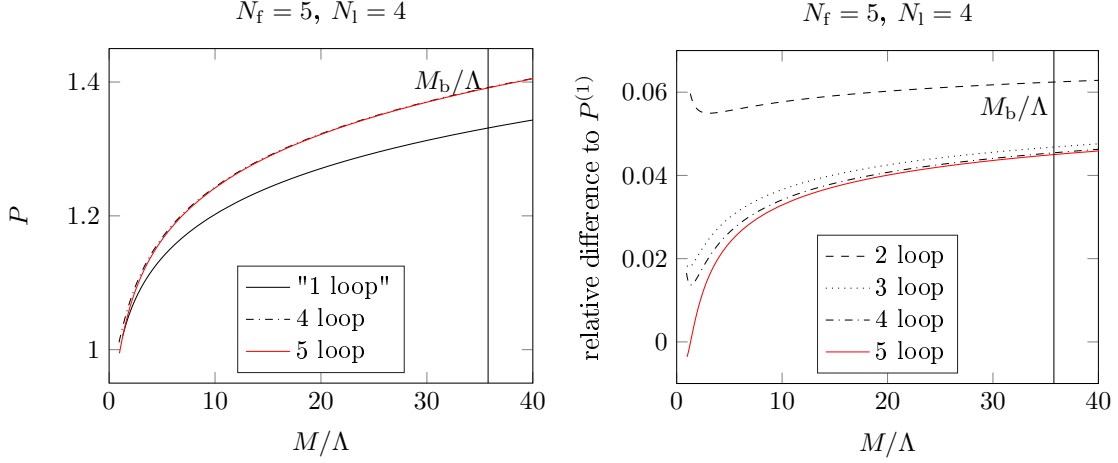


**Figure 7:** The mass-dependence  $P$  at 1-loop formula and at 4,5-loop (left) as well as 2,3,4,5-loop correction normalised to the 1-loop approximation (right) for the case  $N_f = 5, N_l = 4$ .

$N_f$	$N_l$	1 loop	2 loop	3 loop	4 loop	5 loop
2	0	1.2319	1.2546	1.2170	1.2084	-
4	3	1.1448	1.1875	1.1552	1.1492	1.1468
5	4	1.3413	1.4255	1.3947	1.3918	1.3913

**Table 2:** Perturbative values of  $P_{l,f}$  defined in eq. (3.8) for various cases of interest, see main text for details.

all. In table 2 we list the values of  $P$  computed from eq. (3.30) using different orders of perturbation theory. We evaluate  $P$  at an argument  $M/\Lambda$  which depends on  $N_f$  and  $N_l$ . For  $N_f = 2, N_l = 0$  we obtain  $M/\Lambda$  from the PDG value for  $\bar{m}_c$  [20] and  $\Lambda_2 = 310 \text{ MeV}$  from [21]. In this case there is no 5-loop result because the coefficient  $c_4$  is not known. For  $N_f = 4, N_l = 3$  and  $N_f = 5, N_l = 4$  we use the PDG values for  $M_c/\Lambda$  and  $M_b/\Lambda$  as explained above.

#### 4 Non-perturbative investigation for $N_f = 2 \rightarrow N_l = 0$

We investigate a model, namely QCD with  $N_f = 2$  heavy, mass-degenerate quarks. The decoupling is then  $2 \rightarrow 0$  and the Lagrangian of the effective theory,  $\mathcal{L}_{\text{dec}}$ , is the Yang-Mills one up to  $1/M^2$  corrections. We target the RGI quark mass values (see below)

$$\frac{M_{\text{targ}}}{\Lambda} = 0.59, 1.28, 2.50, 4.87, 5.7781. \quad (4.1)$$

Using  $\Lambda = 310 \text{ MeV}$  from [21] their physical values are approximately  $M_{\text{targ}} = 0.2, 0.4, 0.8, 1.5, 1.8 \text{ GeV}$ . The value  $M_{\text{targ}}/\Lambda = 4.87$  corresponds to the RGI charm quark mass  $M_c$  from [22] in agreement with [20] within the present uncertainties. However, for our model study the exact value is not important.

## 4.1 Low energy observables

In principle any low-energy hadronic scale  $m^{\text{had}}(M)$  can be used to study decoupling, but in practice some choices are far superior to others. Ideally we look for a quantity that is easily non-perturbatively renormalizable, well defined in both full and effective theory, has controllable lattice artifacts, is cheap to compute and can be determined with a high precision. Since in our case the effective theory has no fermionic content, we are restricted to purely gluonic observables. Glueball masses would be natural candidates. However, it is difficult to determine them precisely enough. Hadronic scales derived from the static quark potential fulfill all criteria and have been popular for many years. If  $F(r)$  denotes the force between two static quarks (defined in terms of the fundamental Wilson loop), a distance  $r_x$  can be defined implicitly [13] by choosing a number  $c$  and solving

$$r_x^2 F(r_x) = c. \quad (4.2)$$

The choices  $r_0 \Leftrightarrow c = 1.65$  [13] and  $r_1 \Leftrightarrow c = 1.0$  [23] have become standards. In a lattice calculation the latter has a better statistical precision, but larger lattice artifacts. Moreover we expect decoupling to be more precise for the longer distance,  $r_0$ .

In recent years, these scales have been largely replaced by scales based on the gradient flow [1, 24]. The gauge field  $A_\mu$  is used as an initial condition in a flow equation, that describes the relaxation of a field  $B_\mu$  as a function of a flow time  $t$ .

$$\partial_t B_\mu = D_\nu G_{\nu\mu}, \quad B_\mu|_{t=0} = A_\mu. \quad (4.3)$$

The field strength tensor  $G_{\nu\mu}$  and the covariant derivative  $D_\nu$  are defined in the usual way, but at flow time  $t$ . The crucial observation, that correlators of the  $B_\mu$  fields at finite flow time are renormalized quantities [25], allowed to introduce a family of scales. The definition of scales  $\sqrt{t_0}$  [1],  $\sqrt{t_c}$  and  $w_0$  [14] is based on the dimensionless combination

$$\mathcal{E}(t) = t^2 \left\langle \frac{1}{4} G_{\mu\nu}^a G_{\mu\nu}^a \right\rangle, \quad (4.4)$$

together with

$$\mathcal{E}(t_0) = 0.3, \quad (4.5)$$

$$\mathcal{E}(t_c) = 0.2, \quad (4.6)$$

$$w_0^2 \mathcal{E}'(w_0^2) = 0.3. \quad (4.7)$$

In our simulations we compute the hadronic scales

$$m^{\text{had}}(M) = \frac{1}{r_0}, \frac{1}{\sqrt{t_0}}, \frac{1}{\sqrt{t_c}}, \frac{1}{w_0}. \quad (4.8)$$

The rest of this section contains technical details about the lattice simulations. It can be omitted if one is only interested in the physical results presented in section 5.

## 4.2 Fixing the RGI parameters of the theory and details of the simulations

### 4.2.1 Discretization

We use Wilson's plaquette gauge action [26] and include quarks treated with two discretizations:  $O(a)$  improved Wilson fermions [27, 28] and twisted mass [29] Wilson fermions at

maximal twist. For both actions the clover term [27, 28] has the non-perturbatively determined improvement coefficient  $c_{\text{sw}}$  [30]. Twisted mass fermions at maximal twist are automatically  $\mathcal{O}(a)$  improved [31] also without a clover term. However, with the clover term added our two discretizations have a common chiral limit in a finite volume (see  $L_1$  below). Furthermore the clover term reduces  $\mathcal{O}(a^2)$  lattice artifacts as it was shown for example in [32].

In appendix C we list the ensembles generated with standard Wilson fermions in table 4 and with twisted mass Wilson fermions in table 5. The twisted mass simulations are the same as in [33].

We determine the lattice spacings through the scale  $L_1$  [21, 34], which is defined by  $\bar{g}_{\text{SF}}^2(L_1) = 4.484$  through the so-called Schrödinger Functional coupling at zero quark mass and in a finite volume of size  $L_1^4$ . Note that in this situation the two discretizations are identical. Thus at a given gauge coupling  $\beta = 6/g_0^2$  they have one and the same lattice spacing. The values of  $L_1/a$  and the corresponding lattice spacings are listed in table 6.

#### 4.2.2 $\mathcal{O}(a)$ improvement and finite size effects

$\mathcal{O}(a)$  improvement of quark mass effects requires to keep the improved bare coupling  $\tilde{g}_0^2 = (1 + b_g(N_f) am_q) g_0^2$  fixed, where  $m_q = 1/(2\kappa) - 1/(2\kappa_c)$  is the bare subtracted standard mass. Twisted mass fermions at maximal twist have  $m_q = 0$  and therefore the improved coupling is  $\tilde{g}_0 = g_0$ . Instead our simulations with standard Wilson fermions were done at fixed  $g_0$  (and not  $\tilde{g}_0$ ). We correct for the resulting  $\mathcal{O}(am)$  effects in the lattice spacing by decreasing the values of  $am^{\text{had}}(M)$  using the 1-loop result  $b_g(N_f) = 0.01200 N_f g_0^2$  [35, 36] and the 1-loop  $\beta$ -function. For  $m^{\text{had}} = 1/\sqrt{t_0(M)}$  these effects shift the value of  $\sqrt{t_0(M)}/a$  according to

$$\left. \frac{\sqrt{t_0(M)}}{a} \right|_{\tilde{g}_0} \approx \left. \frac{\sqrt{t_0(M)}}{a} \right|_{g_0} \times \left[ 1 + \frac{0.01200 N_f}{2b_0(N_f)} am_q \right]. \quad (4.9)$$

We use  $am_q = am/(Zr_m)$  and the factor  $Zr_m$  is taken from [21] (at  $6/g_0^2 = 5.7$  we get  $Zr_m = 1.194$  from a Padé fit). Here  $am$  denotes the PCAC mass. We added in quadrature 100% of the correction to the errors as an estimate of unknown  $\mathcal{O}(g_0^4)$  terms in  $b_g$ . After the corrections the values of  $am^{\text{had}}(M)$  correspond to simulations performed at  $\beta = 6/\tilde{g}_0^2$ .

Our volumes are such that the lightest pseudo-scalar mass times the box size is  $m_{\text{PS}}L \geq 7.4$  and  $L/\sqrt{t_0(M)} \geq 12$  and  $L/r_0(M) \geq 3.8$ . At our largest masses the situation is comparable to the pure gauge theory, where significant finite volume effects can be excluded for a lattice size  $L \approx 4r_0 = 2.0\text{fm}$ . Approximate decoupling of the heavy quarks means that also our finite mass simulations are practically free of finite volume effects.

#### 4.2.3 Quark masses

Before taking the continuum limit, we non-perturbatively fix the value of the RGI quark mass  $M$  in units of the  $\Lambda$  parameter through the following steps. We take the  $\Lambda$  parameter to be defined in the  $\overline{\text{MS}}$  scheme while the RGI mass  $M$  is independent of the scheme.

In the case of standard Wilson fermions the renormalized quark mass in lattice units  $a\bar{m}_{\text{SF}}(L_1)$  at length scale  $L_1$  is defined by  $a\bar{m}_{\text{SF}}(L_1) = Z_A/Z_P(L_1) am$ , where the renormalisation factor  $Z_P(L_1)$  is defined in the Schrödinger Functional scheme as in [21] and also the details of the definition of  $m$  are found there. The axial current renormalization

factor,  $Z_A$ , is fixed by a chiral Ward identity [37]<sup>1</sup>. For the determination of the PCAC mass  $am$  we use our publicly available program<sup>2</sup>. The ratio  $M/\Lambda$  is then obtained from

$$\frac{M}{\Lambda} = a\bar{m}_{\text{SF}}(L_1) \times M/\bar{m}_{\text{SF}}(L_1) \times \frac{(L_1/a)}{(\Lambda L_1)}, \quad (4.10)$$

where we take  $M/\bar{m}_{\text{SF}}(L_1) = 1.308(16)$  from [21, 39] and  $\Lambda L_1 = 0.649(45)$  from [40]. The values of the PCAC mass  $m$  and of  $M/\Lambda$  are tabulated in table 4. The accuracy of  $M/\Lambda$  is around 7% with an error dominated by the one of  $\Lambda L_1$ . Thus, ratios of masses  $M_1/M_2$  or equivalently logarithmic derivatives with respect to masses are known significantly more precisely.

In the case of twisted mass fermions at maximal twist the difference is that the renormalized quark mass  $a\bar{m}_{\text{SF}}(L_1)$  is calculated through  $a\bar{m}_{\text{SF}}(L_1) = a\mu/Z_P(L_1)$ , where  $a\mu$  is the twisted mass parameter. The ratio  $M/\Lambda$  is again obtained from eq. (4.10). For twisted mass fermions we actually invert eq. (4.10) to determine the twisted mass parameter corresponding to given values of  $M/\Lambda$  which are tabulated in table 5.

#### 4.2.4 Hadronic scales on the lattice

In our simulations we measure the observables discussed in section 4.1. Various details concerning their computation in the discretized theory are as follows.

The clover (symmetric) definition of the action density  $E$  is used in eq. (4.4) and we use the Wilson-flow equation, cf. [1].

The scale  $r_0$  is defined with the “HYP2” action for the static quarks [41]. It is determined with our publicly available program<sup>3</sup> following the details explained in Ref. [42]. We use a variational basis with up to four levels of spatial HYP smearing [43] to construct a matrix of Wilson loops. Due to the open boundary conditions, Wilson loops are averaged only in a temporal region sufficiently far away from the boundaries to exclude contaminations from boundary effects. The static potential as a function of  $r$  is obtained by solving the generalised eigenvalue problem as discussed in Ref. [42].

Hadronic scales such as  $t_0$  are non-linear functions of one or more Monte-Carlo averages of “primary observables”  $\langle\mathcal{O}_1\rangle, \dots, \langle\mathcal{O}_{N_{\text{ob}}}\rangle$ , like for instance the action densities at different flow times. The derivative of such a function with respect to the twisted mass, as needed for the MC evaluation of  $\eta^{\text{M}}$  (below in eq. (5.6)), is in general given by

$$\frac{df(\langle\mathcal{O}_1\rangle, \dots, \langle\mathcal{O}_{N_{\text{ob}}}\rangle, \mu)}{d\mu} = \sum_{i=1}^{N_{\text{ob}}} \frac{\partial f}{\partial \langle\mathcal{O}_i\rangle} \frac{d\langle\mathcal{O}_i\rangle}{d\mu} + \frac{\partial f}{\partial \mu} \quad (4.11)$$

and the derivative of a primary observable  $\mathcal{O}$ ,

$$\frac{d\langle\mathcal{O}\rangle}{d\mu} = -\left\langle \frac{dS}{d\mu} \mathcal{O} \right\rangle + \left\langle \frac{dS}{d\mu} \right\rangle \langle\mathcal{O}\rangle + \left\langle \frac{d\mathcal{O}}{d\mu} \right\rangle. \quad (4.12)$$

For most observables  $\frac{\partial f}{\partial \mu}$  and  $\frac{d\mathcal{O}}{d\mu}$  are absent. The derivative of the action is given by  $dS/d\mu = ia^4 \sum_x \bar{\psi}(x) \gamma_5 \tau^3 \psi(x)$ . In cases like ours, where the observables do not contain

<sup>1</sup> A more precise determination of  $Z_A$  became recently available [38].

<sup>2</sup> It is available at <https://github.com/to-ko/mesons>.

<sup>3</sup> It is available at <https://github.com/bjoern-leder/wloop>.



fermionic fields, no new Wick contractions arise in the first term, and one simply needs to determine the observable and the action-derivative on each configuration and compute their connected correlation. For the action-derivative we write (cf. [44])

$$\begin{aligned}\left\langle \frac{dS}{d\mu} \right\rangle &= ia^4 \sum_x \left\langle \text{tr} [(D_d(x, x)^{-1} - D_u^{-1}(x, x))\gamma_5] \right\rangle^{\text{gauge}} \\ &= -2\mu a^8 \sum_{x,y} \left\langle \text{tr} [D_u^{-1\dagger}(x, y) D_u^{-1}(x, y)] \right\rangle^{\text{gauge}},\end{aligned}\quad (4.13)$$

where in the last step a property of the twisted mass Dirac operators  $D_{u,d}$  (for up and down quark),  $D_u - D_d = 2i\gamma_5\mu$ , was exploited, leading to an expression that has a smaller variance, when the trace is estimated stochastically. A stochastic estimation is necessary to avoid a full matrix inversion, and amounts to solving equations  $D_u\xi = \eta$ , with 4D noise spinors  $\eta$ , for  $\xi$  and a subsequent dot product  $\xi \cdot \xi$ . We find that different noise distributions (e.g. normal or  $U(1)$ -noise) yield a similar variance, and further refinements like spin or color dilution [45] do not pay off. Not many noise-sources are needed for the final error to be close to the limiting error due to gauge field fluctuations. In our measurements we settle for 64  $U(1)$  noise spinors per configuration.

#### 4.2.5 Simulation algorithms

In the case of standard Wilson fermions, part of the simulations are performed using periodic boundary conditions (except for anti-periodic boundary conditions in temporal direction for the fermions) and the MP-HMC algorithm [46]. In order to avoid the freezing of the topological charge (see also next section), for simulations with  $t_0/a^2 > 5.5$  [47, 48] we adopt open boundary conditions in time and use the publicly available openQCD package<sup>4</sup> [49]. We set the boundary improvement coefficients to their tree-level values  $c_G = 1$  and  $c_F = 1$ . In both cases the fermion determinant is Hasenbusch-factorized [50] using a splitting in two factors, thus two pseudo-fermion fields are needed and a hierarchical numerical integrator is employed (Leapfrog and Omelyan-Mryglod-Folk integrator schemes are used at the different levels). The trajectory length is always set to 2.0 and configurations and measurements are separated by at least four trajectories. Most computer resources are spent in the solution of the Dirac equation with the smallest mass. For  $M/\Lambda > 1$  we use the SAP preconditioned GCR algorithm [51] while for  $M/\Lambda < 1$  it is profitable to use a multigrid solver [52], which is implemented as the two-grid “locally deflated” solver in the openQCD package since version 1.2. The cost of the simulations is low compared to simulations in the chiral regime.

In the case of twisted mass fermions we use a version of openQCD, in which the SAP preconditioner can have a different value of  $\mu$  than the simulated one. In the preconditioner the twisted mass term is defined only on the even sites. We achieve a significant speed up of the SAP preconditioned GCR algorithm by choosing a value of  $\mu$  for the SAP preconditioner which is larger by approximately a factor 6 than the simulated one (the multi-grid inverter of [53] implements a similar strategy inspired by our findings).

Open boundary conditions are used as specified above. In this setup the Wilson–Dirac operator has two mass parameters, the standard bare quark mass  $m_0$  and the twisted mass

<sup>4</sup> <http://luscher.web.cern.ch/luscher/openQCD/>

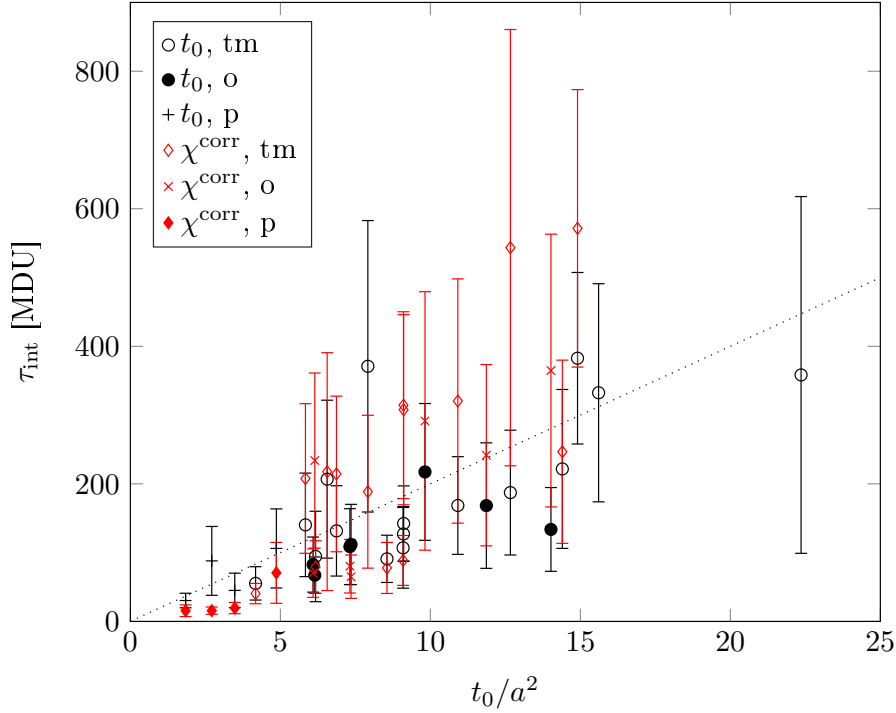


**Figure 8:** Autocorrelation times derived from observables which are expected to have large overlap with the slowest modes in the simulation are plotted as a function of  $t_0(M)/a^2$ . The dotted line represents eq. (4.15).

$\mu$ . Maximal twist means that  $m_0$  is set to its critical value  $m_c$  which corresponds to the vanishing of the current (PCAC) quark mass. We extracted the critical mass from table 13 in [21], interpolating the data to the desired  $\beta$  values by a Padé fit in  $g_0^2 = 6/\beta$  of the form

$$am_c(g_0) = u_1 g_0^2 + g_0^4 \frac{\sum_{k=0}^3 u_{2+k} g_0^{2k}}{1 + u_d g_0^2} \quad (4.14)$$

where the coefficients  $u_1$  and  $u_2$  coincide with two-loop perturbation theory [54]. The values of the hopping parameter  $\kappa = 1/(2am_c + 8)$  are listed in table 5.

#### 4.2.6 Autocorrelation times and error analysis

We measure the integrated autocorrelation time  $\tau_{\text{int}}$  for all measured quantities including the hadronic scales, the PCAC mass and additionally the topological susceptibility. We find the largest  $\tau_{\text{int}}$  for the scale  $t_0$  and for the topological susceptibility  $\chi^{\text{corr}}$  as defined in [48], see figure 8, which we use as a rough estimate of the exponential autocorrelation time  $\tau_{\text{exp}}$ , cf. [47].

At the smallest lattice spacing  $a = 0.036$  fm that we reach with standard Wilson fermions we estimate  $\tau_{\text{exp}} \simeq 200 - 300$  MDU (Molecular Dynamics Units). Our statistics of 4000 – 8000 MDU is therefore adequate but does require a particularly careful error analysis. With twisted mass fermions at maximal twist we reach a smallest lattice spacing of  $a = 0.023$  fm ( $\beta = 6.0$ ). There we estimate  $\tau_{\text{exp}} = 357$  MDU and have a statistics of

$63\tau_{\text{exp}}$ . For the twisted mass simulations at  $M/\Lambda = 4.87$  and  $\beta = 5.88, 6.0$  the statistics is too small to determine  $\tau_{\text{int}}$  for  $\chi^{\text{corr}}$ . The autocorrelation times shown in figure 8 are reasonably well described by the dotted line

$$\tau_{\text{exp}} = 20t_0/a^2, \quad (4.15)$$

where one has to take into account that determinations of  $\tau_{\text{exp}}$  including an error estimate are notoriously difficult. Thus the data in figure 8 is consistent with the expectation, that for simulations with open boundary conditions autocorrelation times scale with  $1/a^2$ .

The error analysis is performed with the program<sup>5</sup> of [47]. It is based on [55] and adds a tail to the autocorrelation function as an estimate of the slow mode contribution [47].

## 5 Non-perturbative mass dependence

### 5.1 Test of the factorization formula

We remind that our model is QCD with two heavy, mass-degenerate quarks and thus the effective theory, decQCD, is the Yang-Mills theory up to  $1/M^2$  corrections ( $N_f = 2$ ,  $N_1 = 0$ ). For the hadronic scale  $m^{\text{had}} = 1/\sqrt{t_0}$  [1], the factorization formula eq. (3.12) takes the form

$$\sqrt{\frac{t_0(M)}{t_0(0)}} = \frac{1}{Q_{0,2}^{\sqrt{t_0}} \times P_{0,2}(M/\Lambda)} + \mathcal{O}((\Lambda/M)^2) \quad (5.1)$$

with  $Q_{0,2}^{\sqrt{t_0}} = [\Lambda\sqrt{t_0(0)}]_{N_f=2}/[\Lambda\sqrt{t_0}]_{N_f=0}$ . We turn now to a comparison of eq. (5.1) to non-perturbative data. Preliminary results have been presented in [56], where only data for Wilson fermions were available. Now we can combine those data with the new simulations with twisted mass fermions and perform careful continuum extrapolations. In the extrapolations we only use data points which satisfy  $a^2/t_0(M) < 0.32$ .

In order to compute the ratio in eq. (5.1) we write

$$\sqrt{\frac{t_0(M)}{t_0(0)}} = \frac{\sqrt{t_0(M)}}{L_1} \times \left( \frac{\sqrt{t_0(0)}}{L_1} \right)^{-1} \quad (5.2)$$

and separately take continuum limits for the two factors on the right hand side. There the mass independent scale  $L_1$  enters, see section 4. The pairs  $(L_1/a, \beta)$  are computed from a quadratic fit of  $\ln(L_1/a)$  as a function of  $\beta$ . We take data for  $L_1/a$  from table 13 of [21] and add the newly determined values  $L_1/a = 20.31(69)$  at  $\beta = 6.1569$  and  $L_1/a = 24.83(88)$  at  $\beta = 6.2483$ .

The first factor on the right hand side of eq. (5.2) is computed using the data  $t_0(M)/a^2$  obtained in the simulations listed in table 4 and table 5. For the simulations with standard Wilson fermions we include the  $b_g$  effects as explained in section 4.2.2. We have data for five values of the quark masses given in eq. (4.1). Some of our data for the ratio  $\sqrt{t_0(M)}/L_1$  are shown in the right plot of figure 9 together with their continuum extrapolations. We show the two extreme values of the quark mass, separated by a factor of 8. The extrapolations linear in  $a^2/t_0$  work very well and we observe that the size of cut-off effects is smaller for

<sup>5</sup> <http://www-zeuthen.desy.de/alpha/>

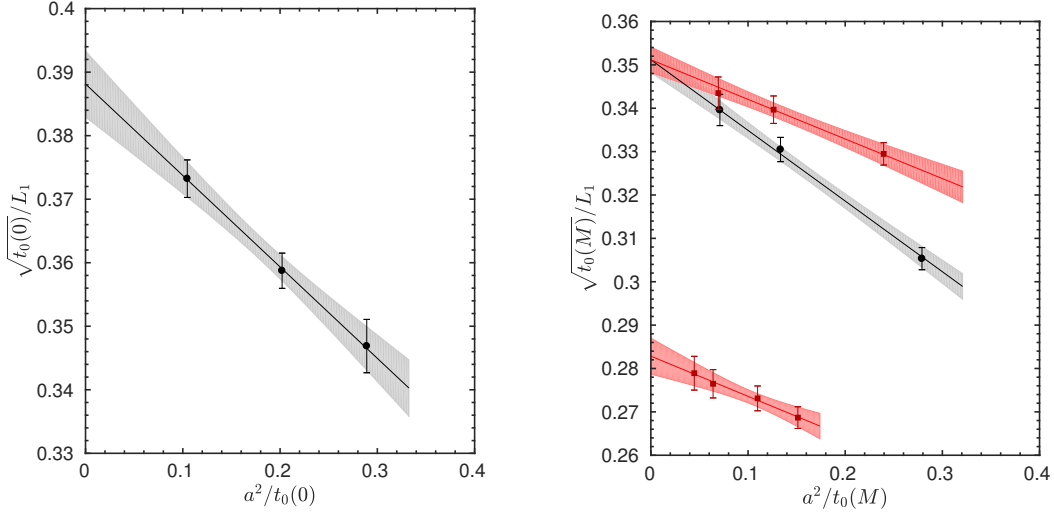


**Figure 9:** Continuum extrapolations of  $\sqrt{t_0}/L_1$ , using a linear extrapolation in  $a^2/t_0(M)$ . The shaded bands are the extrapolation errors. The left plot shows the results for  $\sqrt{t_0(0)}$  in the chiral limit. The right plot shows the results for  $\sqrt{t_0(M)}$  at  $M/\Lambda = 0.59$  (upper data set in the plot) and  $M/\Lambda = 4.87$  (the charm quark mass  $M_c$ , lower data set in the plot). Black circles represent the standard Wilson and red squares the twisted mass discretizations. Where both are available a combined continuum extrapolation is performed.

the twisted mass data. For this reason we opted for the twisted mass discretization to simulate masses at or larger than the charm quark mass.

In order to compute the second factor on the right hand side of eq. (5.2) we use the values of  $t_0(0)/a^2$  in the chiral limit which are known for  $\beta = 6/g_0^2 = 5.2, 5.3$  and  $5.5$  from [16]. The continuum extrapolation of  $\sqrt{t_0(0)}/L_1$  linear in  $a^2/t_0(0)$  using the three  $\beta$  values works well, see the left plot of figure 9 and yields  $\sqrt{t_0(0)}/L_1 = 0.3881(52)$ .

Our continuum results for the ratio  $\sqrt{t_0(M)}/t_0(0)$  are listed in table 3. Correlations of the two factors originating from the common data of the scale  $L_1/a$  help to reduce the overall error.

Figure 10 shows the values of  $\sqrt{t_0(M)}/t_0(0)$  of table 3 as a function of  $\Lambda/(\Lambda + M)$ . We display a horizontal error stemming from the uncertainty of  $M/\Lambda$  originating from  $\Lambda L_1$  in eq. (4.10). The vertical dotted lines mark the values of the quark mass  $M_c$ ,  $M_c/2$  and  $M_c/4$ . We compare the Monte Carlo data to the factorization formula eq. (5.1), where the factor  $P_{0,2}$  is computed to 2- (blue dashed line) and 4-loops (black line). The error on the factorization formula comes from the numerical values  $[\Lambda L_1]_{N_f=2} = 0.629(36)$  [21],  $[\sqrt{t_0}/L_1]_{N_f=2} = 0.3881(52)$ ,  $[\Lambda r_0]_{N_f=0} = 0.602(48)$  [57],  $[\sqrt{t_0}/r_0]_{N_f=0} = 0.3319(19)$  [33] combined to

$$Q_{0,2}^{\sqrt{t_0}} = \frac{[\Lambda L_1]_{N_f=2} \times [\sqrt{t_0}/L_1]_{N_f=2}}{[\Lambda r_0]_{N_f=0} \times [\sqrt{t_0}/r_0]_{N_f=0}} = 1.22(12) \quad (5.3)$$

and is displayed by the gray shaded band only for the 4-loop curve. For completeness,

$M/\Lambda$	$\sqrt{t_0(M)/t_0(0)}$
0.5900	0.9048( 43)
1.2800	0.8458( 74)
2.5000	0.7880( 73)
4.8700	0.7287(127)
5.7781	0.7151(102)

**Table 3:** The values of  $\sqrt{t_0(M)/t_0(0)}$  computed through eq. (5.2). The errors are obtained from error propagation which takes into account the correlation between the two factors in eq. (5.2).

in figure 10 the magenta line to the right shows the mass dependence in the chiral limit estimated from [15, 16], cf. [58].

From figure 10 we see that there is agreement between the Monte Carlo data of table 3 and the factorization formula eq. (5.1) for quark masses at the charm quark mass value  $M_c$ . Thus within our precision of 10% due to the uncertainty of the factor  $Q$  in eq. (5.3), the data match the upper error band of the perturbative prediction. In [11] we presented results for the ratio  $r_0(M)/r_0(0)$  and reached similar conclusions albeit with less precise data covering only the region below the charm quark mass. Our new results for  $\sqrt{t_0(M)/t_0(0)}$  are much more precise than the value of  $Q$  extracted from the literature. This allows to turn the tables and predict

$$Q_{0,2}^{\sqrt{t_0}} = 1.134(17), \quad (5.4)$$

obtained by taking  $M/\Lambda = 5.7781$  in eq. (5.1). For  $\sqrt{t_0(M)/t_0(0)}$  we use our result in the last line of table 3. We evaluate the factor  $P_{0,2}(M/\Lambda = 5.7781) = 1.2328$  and assign to it a 0.4% error as it will be estimated in section 6. This determination avoids entirely the computation of the running of the coupling at high energy [40, 57]. In a nutshell it is replaced by perturbation theory for the difference of the running. The essential point is that the latter is given by the contribution of quark loops for which we non-perturbatively confirm that perturbation theory is very accurate. We will comment more on this in the conclusions.

## 5.2 The mass-scaling function $\eta^M$

By discretizing the derivative in eq. (3.15) we obtain from our simulations numerical estimates of the mass-scaling function

$$\eta^M(\overline{M}) \approx \frac{\log(m^{\text{had}}(M_2)/m^{\text{had}}(M_1))}{\log(M_2/M_1)}, \quad \overline{M} = \sqrt{M_2 M_1}. \quad (5.5)$$

We use this definition to compute  $\eta^M(\overline{M})$  at  $\overline{M} = \sqrt{1.28 \times 0.59}$  and  $\sqrt{2.50 \times 1.28}$  using  $m^{\text{had}} = 1/\sqrt{t_0}$ ,  $1/\sqrt{t_c}$  and  $1/w_0$ . As emphasized before, these estimates differ by  $1/M^2$  effects. We have data at three values of the lattice coupling  $\beta = 6/g_0^2 = 5.3, 5.5$  and  $5.7$  for both standard Wilson and twisted mass discretizations. We can also compute a value of  $\eta^M(\overline{M})$  at  $\overline{M} = \sqrt{4.87 \times 5.7781}$  but its statistical errors are large.

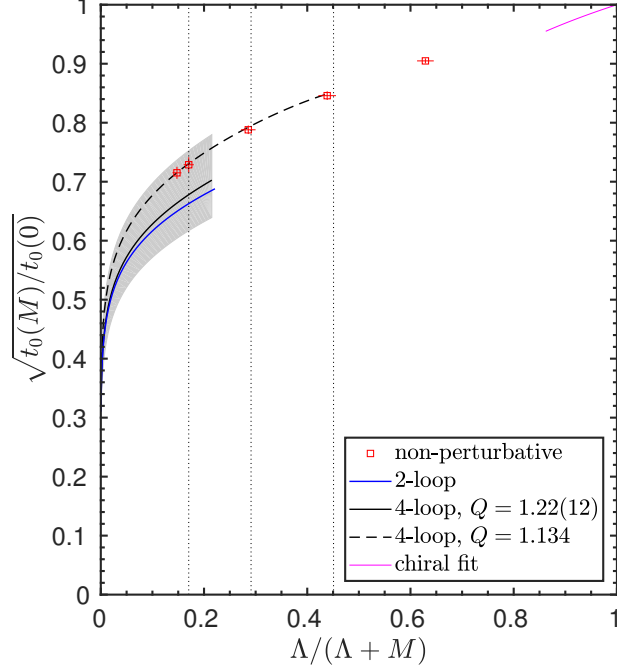


**Figure 10:** The mass-dependence of the ratio  $\sqrt{t_0(M)/t_0(0)}$  in the theory with two mass-degenerate quarks. Monte Carlo data after continuum extrapolation are compared with the perturbative predictions for  $1/(QP)$  at large  $M$  eq. (5.1). The gray shaded error band represent the error of the 4-loop curve (black line) deriving from  $Q$ . The dashed line is the 4-loop curve adjusting the value of  $Q$  to go through the point at  $M/\Lambda = 5.7781$ , see eq. (5.4). A fit function which describes the mass-dependence close to the chiral limit is also shown to the right. The vertical dotted lines mark the values of the quark mass  $M_c$ ,  $M_c/2$  and  $M_c/4$ .

For the case  $m^{\text{had}} = 1/\sqrt{t_0}$  and  $\overline{M} = \sqrt{1.28 \times 0.59}$ , the simulation data are shown in the left plot of figure 11. The continuum value results from a combined continuum extrapolation linear in  $a^2/t_0^2$ . In all our continuum extrapolations we apply the cut  $a^2/t_0(M) < 0.32$  to the data to be fitted. The plot shows the continuum extrapolation for both discretizations together with its error bands.

The continuum values of  $\eta^M(\overline{M})$  for the various choices of  $m^{\text{had}}$  are presented in figure 12 and plotted against  $1/(1 + (\overline{M}/\Lambda)^2)$ . Notice that the data points corresponding to different quantities  $m^{\text{had}}$  are slightly displaced horizontally for clarity of presentation. The spread of the data due to  $1/M^2$  effects decreases when  $\overline{M}$  increases as expected. For comparison we plot in figure 12 also the 1-loop (the constant value  $\eta_0$ ) and 4-loop (up to the  $\eta_3^M$  term) expressions, see eq. (3.25), eq. (3.26) and appendix A.

The mass-scaling function  $\eta^M$  can also be computed directly from a simulation at a

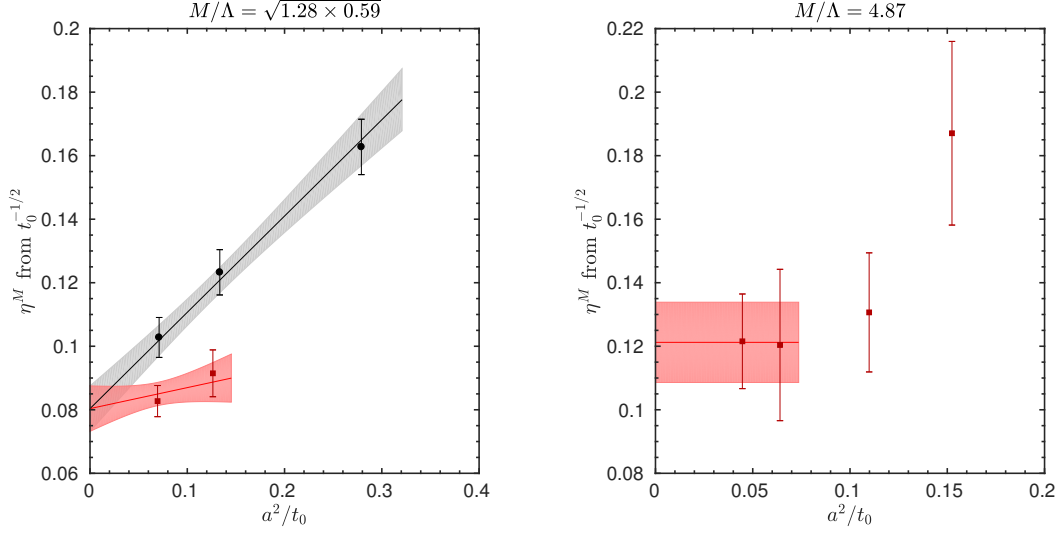


**Figure 11:** Examples of continuum limits of  $\eta^M(M)$  extracted from  $m^{\text{had}} = 1/\sqrt{t_0}$  using a linear extrapolation in  $a^2/t_0(M)$ . In the left plot  $\eta^M(\bar{M})$  is computed at  $\bar{M}/\Lambda = \sqrt{1.28 \times 0.59}$  using the definition eq. (5.5). Shown are data for standard Wilson (black circles) and twisted mass (red squares) and their combined continuum extrapolation. In the right plot  $\eta^M(M)$  is computed at  $M = M_c$  ( $M/\Lambda = 4.87$ ) using the definition eq. (5.6).

single quark mass. Using the twisted mass discretization we can rewrite eq. (3.15), for example taking  $m^{\text{had}} = 1/\sqrt{t_0}$ , as

$$-\frac{\mu}{2t_0} \frac{dt_0}{d\mu} = \eta^M(M). \quad (5.6)$$

The derivative  $\frac{dt_0}{d\mu}$  is computed as explained in section 4.2.4. Using  $m^{\text{had}} = 1/\sqrt{t_c}$  or  $1/w_0$  results in determinations of  $\eta^M(M)$  similar to eq. (5.6).

In the right plot of figure 11 we show the data for the quantity on the left-hand side of eq. (5.6) computed from our simulations at  $M = M_c$  ( $M/\Lambda = 4.87$ ) with twisted mass fermions at four values of the lattice coupling  $\beta = 6/g_0^2 = 5.6, 5.7, 5.88$  and  $6.0$ . Our fine lattices are needed to control the cut-off effects at this large value of the mass. We perform continuum extrapolations by “fits” to a constant. Taking three, two or just the last point yields results which are in agreement. We settle for the two-point average which of course has a larger error than the three-point one. The continuum values are plotted in figure 12, together with similar determinations of  $\eta^M(M_c)$  from  $m^{\text{had}} = 1/\sqrt{t_c}$  and  $1/w_0$ . At  $M = M_c$  the different determinations agree well with each other signaling the smallness of the  $1/M^2$  corrections [33].

For our model with two charm quarks we see from figure 12 that  $\eta^M$  is about  $1/10$ , both in perturbation theory and non-perturbatively. For a single charm quark there is an additional factor  $1/2$ . Thus a 2% shift of the charm quark mass leads only to a 1‰ change of a low energy hadronic quantity of mass-dimension one.

The precision of  $\eta^M(M_c)$  that we can achieve is around 10%. Within this error the non-

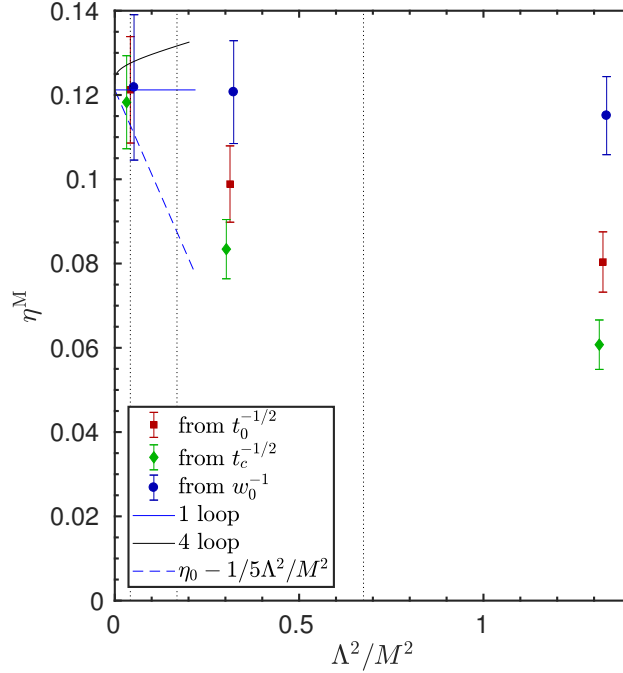


**Figure 12:** The mass dependence of the mass-scaling function  $\eta^M$  in the theory with two mass-degenerate quarks.  $\eta^M$  is obtained from the hadronic scales  $1/\sqrt{t_0}$ ,  $1/\sqrt{t_c}$  and  $1/w_0$  and the data for a given mass  $M$  are slightly displaced horizontally for clarity. The Monte Carlo data are compared to the perturbative curves. The vertical dotted lines mark the values of the quark mass  $M_c$ ,  $M_c/2$  and  $M_c/4$ .

perturbative values agree with the perturbative one. This does not look very precise, but in absolute terms this is  $\Delta\eta^M = 0.01$ . We put this into the perspective of phenomenology in the following section.

## 6 How big are the effects of charm loops?

We recapitulate that the effects of charm loops at low energies come in two classes. One is when we are concerned with dimensionless low energy observables which do not refer to quantities at energies around or above the charm mass. In lattice slang: the quantity is long distance and the lattice spacing  $a$  is set through long distance physics in the theory with the heavy quark. In this case the value of the  $\Lambda$ -parameter drops out and the only effects of the heavy quark mass are due to the power corrections originating from  $\mathcal{L}_2$  studied in [11, 33]. These effects are very small. To be specific, when decoupling two charm quarks, the power corrections in ratios of hadronic scales eq. (4.8) were found to be approximately 0.4%.

The prototype for the second class is given by the connection of the fundamental scales



of the four-flavor and the three-flavor theory. In our model it is the connection between the two-flavor theory and the zero-flavor theory. The very relevant question is what the uncertainty is when one uses the perturbatively computed  $P_{1,f}(M/\Lambda_f)$ . In section 3.3 we have seen that 3,4,5-loop corrections are very small. How big can non-perturbative effects be? The close agreement of our non-perturbative  $\eta^M$  (section 5.2) with perturbation theory and the dashed curve in figure 10 with the non-perturbative points shows that they are small. We now put this into numbers.

In figure 12 we included a dashed curve corresponding to  $\eta^M = \eta_0 + c \frac{\Lambda^2}{M^2}$  as a very crude model for non-perturbative effects. The term  $\frac{\Lambda^2}{M^2}$  is the leading non-perturbative effect due to  $\mathcal{L}_2$  and we add  $\eta_0$  to have the correct asymptotics. Adding higher order perturbative terms seems beyond this semiquantitative consideration. We chose  $c = -1/5$ , which is a relatively large coefficient if the behavior at  $\frac{\Lambda^2}{M^2} \approx 0.3$  can be compared to the charm region; Covering the end of the error bars at the charm would require a somewhat larger  $|c|$ . The effect of the  $\frac{\Lambda^2}{M^2}$  term on  $P_{1,f}(M/\Lambda_f)$  is easily evaluated. We write

$$\eta^M = \eta_{\text{pert}}^M + \eta_{\text{NP}}^M, \quad (6.1)$$

where  $\eta_{\text{pert}}^M$  may be the 4-loop expression and  $\eta_{\text{NP}}^M$  the rest, which depends on  $\mathcal{Q}$ . We want to estimate its effect on  $P_{1,f}(M/\Lambda_f)$  and for that purpose choose

$$\eta_{\text{NP}}^M = c \frac{\Lambda^2}{M^2}. \quad (6.2)$$

We then have  $\log(P) = \int^{\log(M/\Lambda)} h(x) dx$  with  $x = \log(M/\Lambda)$  and  $\eta^M = h(x)$ . The non-perturbative part is  $h_{\text{NP}}(x) = c e^{-2x}$ . Fixing the integration constant by the perturbative expression (at arbitrarily high  $M$ ), we find

$$\Delta \log [P_{1,f}(M/\Lambda_f)] \equiv \log [P_{1,f}(M/\Lambda_f)] - \log [P_{1,f}(M/\Lambda_f)|_{\text{pert}}] = -\frac{c}{2} \frac{\Lambda^2}{M^2}. \quad (6.3)$$

Inserting our sensical  $c = -1/5$  and the approximate charm mass value  $\frac{\Lambda^2}{M_c^2} \approx 1/25$  yields  $\Delta \log [P_{1,f}(M/\Lambda_f)] = 0.004$ .

This means a 0.4% change (or better uncertainty) due to non-perturbative effects of the described form and magnitude. In other words a 0.4% precision for perturbation theory in the conversion of the  $\Lambda$ -parameter!

## 6.1 Heavy quark content of the nucleon

The matrix element of the scalar heavy quark density between nucleon states is a relevant contribution to the cross-section for the scalar interaction of dark matter with ordinary matter [59]. It can be related, by the Hellmann–Feynman theorem, to the derivative of the nucleon mass  $m_N$  with respect to the heavy quark mass. In the chiral limit for the up, down and strange quark and up to  $O(\Lambda^2/M_q^2)$  this derivative is the mass-scaling function  $\eta^M$ , see eq. (3.15),

$$\frac{1}{m_N} \langle N | m_{q,0} (\bar{q}q)_0 | N \rangle = \frac{1}{m_N} \langle N | M_q (\bar{q}q)_{\text{RGI}} | N \rangle = \eta^M + O(\Lambda^2/M_q^2), \quad (6.4)$$

where  $m_{q,0}$  is the bare heavy quark mass and  $(\bar{q}q)_0$  is the bare scalar density of quark  $q$ , and  $(\bar{q}q)_{\text{RGI}}$  is the RGI-renormalized scalar heavy quark density. Our result in figure 12 shows

that perturbation theory can be safely applied to compute  $\eta^M$  as it was done in [17, 60, 61] and non-perturbative effects in  $\eta^M$  are below 0.004 for the case of a single charm quark as just discussed.

## 6.2 From the model to QCD

Note that currently the precision for the  $\Lambda$ -parameter is at the level of around 4% [20, 62]. This sets the scale for what is small and what is big. Furthermore, there is no reason why our toy-model computation should give a significantly different result for the magnitude (not the details) of non-perturbative effects except that we have decoupled *two* heavy quarks. This leads immediately to the expectation that 1-quark-loop effects, non-perturbative in the gauge coupling, will be about a factor two smaller for the decoupling of the charm-quark in QCD, compared to the model. We use this for the magnitude of all non-perturbative effects, i.e. the uncertainty of perturbation theory.

We conclude that one can *safely* neglect non-perturbative effects all-together for connecting three-flavor and four-flavor  $\Lambda$  at a level down to 1% accuracy. Our results suggest that the accuracy is actually of the order of 0.2%, but the precision for  $\eta^M$  obtained directly at the charm mass as well as the wrong number of light quarks in the model may put that into question. When other sources of uncertainty reach a level below 1% one may want to add a 0.5% uncertainty to the perturbative  $P_{3,4}$  and will still be on the safe side.

In the same way non-perturbative effects to eq. (6.4) are estimated to be below 0.01 in QCD for  $q$  equal to the charm quark.

## 7 Conclusions

In this article we presented a numerical study of the decoupling of heavy quarks. In particular we study the dependence of hadronic, low energy quantities on the mass  $M$  of the decoupled heavy quark. We define and compute in perturbation theory a mass-dependence function  $\eta^M$  eq. (3.15). This computation is performed in leading order in the effective theory which describes the decoupling of the heavy quarks at low energy. We study the behavior of perturbation theory for the function  $\eta^M$  and show that perturbation theory by itself suggests that it is well within the region of asymptotic convergence even for the case of decoupling a charm quark. We remark that  $\eta^M$  can be related to the heavy quark content of the nucleon, see eq. (6.4), which is a relevant input for dark matter searches.

To test the applicability of perturbation theory at the charm quark mass we compare the mass dependence of the ratio  $\sqrt{t_0(M)/t_0(0)}$  defined in terms of the hadronic scale  $1/\sqrt{t_0}$  to the perturbative prediction, see figure 10. We also determine the mass-scaling function  $\eta^M$  non-perturbatively, see figure 12. In order to be able to control the continuum extrapolations and have precise results we do this in a model consisting of two mass-degenerate quarks whose mass ranges up to the charm quark mass. The non-perturbative mass dependence agrees with the perturbative prediction at a level of about 10% for the small mass-scaling function  $\eta^M$  computed at the charm quark mass. This means that we confirm that a 2% shift of the charm quark mass leads only to a 1‰ change of a low energy hadronic quantity of mass-dimension one. We explained in section 6 that this precision is good enough to conclude that at the charm mass, the function  $P_{l,f}$  can be predicted by

perturbation theory with  $\approx 0.2\% \times (N_f - N_1)$  accuracy. This allows to predict

$$\frac{\Lambda_{\overline{\text{MS}}}\sqrt{t_0(0)}\big|_{N_f=2}}{\Lambda_{\overline{\text{MS}}}\sqrt{t_0}\big|_{N_1=0}} = 1.134(17). \quad (7.1)$$

Moreover we estimate that the non-perturbative effects in  $\eta^M$  are below 0.004 for the charm quark.

On the other hand, in the direct comparison of  $\sqrt{t_0(M_c)/t_0(0)}$  to the product  $Q P$ , eq. (3.12) we presently have only 10% accuracy because in the literature the ratio,  $Q$  is not known more precisely.

Our most important conclusion concerns phenomenology: the ratio of three-flavor and four-flavor  $\Lambda$ -parameters can be computed in perturbation theory with an about 0.2% precision. Power corrections  $\sim 1/M_c^2$  were found to be at the same level in low energy observables [11, 33]. Adding a safety margin, this means that the  $\Lambda$ -parameter of the five-flavor theory is safely predicted at the percent level from three-flavor low energy physics once the running of the coupling is under control [63], see section 6.2 for details. Note that the present precision of  $\Delta\alpha_{\overline{\text{MS}}}(M_Z) = 0.0008$  of [63] corresponds to 3.5% in the  $\Lambda$ -parameter. Thus, there is plenty of room for relevant improvement within the three-flavour theory.

Similarly we conclude that non-perturbative effects to the charm quark content of the nucleon, eq. (6.4) are below 0.01.

**Acknowledgement.** We thank M. Bruno and J. Heitger for their inputs for our analyses. We thank M. Dalla Brida and A. Ramos for providing valuable feedback on the manuscript. We gratefully acknowledge the computer resources granted by the John von Neumann Institute for Computing (NIC) and provided on the supercomputer JUROPA at Jülich Supercomputing Centre (JSC) and by the Gauss Centre for Supercomputing (GCS) through the NIC on the GCS share of the supercomputer JUQUEEN at JSC, with funding by the German Federal Ministry of Education and Research (BMBF) and the German State Ministries for Research of Baden-Württemberg (MWK), Bayern (StMWFK) and Nordrhein-Westfalen (MIWF). We are further grateful for computer time allocated for our project on the Konrad and Gottfried computers at the North-German Supercomputing Alliance HLRN, on the CHEOPS, a scientific supercomputer sponsored by the DFG of the regional computing centre of the University of Cologne (RRZK), the Stromboli cluster at the University of Wuppertal and the PAX cluster at DESY, Zeuthen. This work is supported by the Deutsche Forschungsgemeinschaft in the SFB/TR 55 and is based on previous work [11] supported also by the SFB/TR 09. FK thanks CERN for hospitality.

## A Expansion of the matching condition and the mass scaling function

The coefficients of the matching of the coupling (3.17) can be found in [4, 18, 64]. We collect here all known coefficients for convenience. Note that we use the particular scale  $\mu = m_*$ , for which logarithms  $\log(\mu/\bar{m}(\mu))$  vanish and  $c_1 = 0$ . The two loop coefficient is known for arbitrary  $N_f, N_1$

$$c_2 = (N_f - N_1) \frac{11}{72} (4\pi^2)^{-2}, \quad (\text{A.1})$$

The three loop one is known for  $N_f - N_1 = 1, 2$

$$c_3 = [1.881732 - 0.169303 N_1] (4\pi^2)^{-3} \quad \text{for } N_f - N_1 = 2, \quad (\text{A.2})$$

$$c_3 = [0.972057 - 0.084651 N_1] (4\pi^2)^{-3} \quad \text{for } N_f - N_1 = 1, \quad (\text{A.3})$$

and the four loop one only for  $N_f - N_1 = 1$

$$c_4 = [5.170347 - 1.009932 N_1 - 0.021978 N_1^2] (4\pi^2)^{-4} \quad \text{for } N_f - N_1 = 1. \quad (\text{A.4})$$

The coefficients of the expansion of the mass scaling function (3.23) are obtained by expanding (3.21). Up to four loop they are given by

$$\eta_0 = 1 - \frac{b_0(N_f)}{b_0(N_1)}, \quad (\text{A.5})$$

$$\eta_1 = (\eta_0 - 1) [\tilde{b}_1(N_f) - \tilde{b}_1(N_1)], \quad (\text{A.6})$$

$$\eta_2 = (\eta_0 - 1) [c_2 + \tilde{b}_2(N_f) - \tilde{b}_2(N_1)] - \tilde{b}_1(N_1) \eta_1 \quad (\text{A.7})$$

$$\eta_3 = (\eta_0 - 1) [2c_3 + \tilde{b}_3(N_f) - \tilde{b}_3(N_1)] - \tilde{b}_1(N_1) \eta_2 + (c_2 - \tilde{b}_2(N_1)) \eta_1 \quad (\text{A.8})$$

$$\begin{aligned} \eta_4 = (\eta_0 - 1) [3c_4 + \tilde{b}_4(N_f) - \tilde{b}_4(N_1) + \tilde{b}_1(N_f) c_3 - c_2 (4c_2 + \tilde{b}_2(N_1))] \\ - \tilde{b}_1(N_1) \eta_3 + (c_2 - \tilde{b}_2(N_1)) \eta_2 + (c_3 - \tilde{b}_3(N_1)) \eta_1. \end{aligned} \quad (\text{A.9})$$

The evaluation of the coefficients require the knowledge of the  $\beta$ -function of the coupling up to five loops [6–10].

The coefficients of the function (3.25) are straightforwardly obtained from (3.26). Their evaluation requires in addition the anomalous dimension up to four loops [65, 66].

## B Asymptotic expression for $P(M/\Lambda)$

In this section we derive the asymptotic expression eq. (3.28). Starting point is the definition of  $P(M/\Lambda)$  as the ratio of the  $\Lambda$ -parameters. We are interested in the asymptotic behavior at large  $M/\Lambda$ . Since our matching/renormalization scale  $\mu = m_*$  is tied to the mass  $\bar{m}(m_*) = m_*$ , large  $M/\Lambda$  means small  $g_* = \bar{g}(m_*)$ , cf. section 3.2. Therefore we neglect terms  $O(g_*^2)$ . Using eq. (3.1) one obtains (see also eq. (3.30))

$$\log[P(M/\Lambda)] = \log(\Lambda_1/m_*) - \log(\Lambda_f/m_*) \quad (\text{B.1})$$

$$= I_g^1(g_*) \tilde{C}(g_*) - I_g^f(g_*), \quad (\text{B.2})$$

$$= \frac{\eta_0}{2b_0(N_f)g_*^2} - \frac{b_1(N_1)}{2b_0(N_1)^2} \log(b_0(N_1)g_*^2) \quad (\text{B.3})$$

$$+ \frac{b_1(N_f)}{2b_0(N_f)^2} \log(b_0(N_f)g_*^2) + O(g_*^2). \quad (\text{B.4})$$

In order to replace the coupling we extract the asymptotic relation between  $g_*$  and  $M/\Lambda$  from eq. (3.33). Using the shorthands  $\ell = \log(M/\Lambda)$  and  $x = 2b_0(N_f)g_*^2$  the relation up to  $O(g_*^2)$  is

$$\ell = \frac{1}{x} - \frac{d_0}{2b_0(N_f)} \log(x) + \frac{b_1(N_f)}{2b_0(N_f)^2} \log(x/2) + O(x). \quad (\text{B.5})$$

Taking the logarithm on both sides yields  $\log(\ell) = -\log(x) + \mathcal{O}(x \log(x))$ . Inverting gives the result

$$\frac{1}{x} = \ell + \frac{d_0}{2b_0(N_f)} \log(\ell) - \frac{b_1(N_f)}{2b_0(N_f)^2} \log(\ell/2) + \mathcal{O}\left(\frac{\log(\ell)}{\ell}\right). \quad (\text{B.6})$$

Using these relations  $g_*$  can be eliminated from (B.3)-(B.4) and one arrives at eq. (3.28).

## C Simulation parameters

Table 4 and table 5 summarize the parameters of our simulations of  $N_f = 2$  mass-degenerate quarks using  $\mathcal{O}(a)$  improved standard Wilson fermions and twisted mass Wilson fermions at maximal twist respectively.

$\frac{T}{a} \times \left(\frac{L}{a}\right)^3$	$\beta$	BC	$\kappa$	$am$	$M/\Lambda$	$r_0/a$	$t_0/a^2$	kMDU
$64 \times 32^3$	5.3	p	0.13550	0.03405(8)	0.638(46)	5.903(36)	3.481(14)	1
$64 \times 32^3$	5.3	p	0.13450	0.06979(7)	1.308(95)	5.193(20)	2.714(14)	2
$64 \times 32^3$	5.3	p	0.13270	0.13873(8)	2.600(189)	4.270(6)	1.842(3)	2
$120 \times 32^3$	5.5	o	0.136020	0.02467(4)	0.630(46)	8.49(12)	7.318(36)	8
$120 \times 32^3$	5.5	o	0.135236	0.05022(3)	1.282(93)	7.580(44)	6.092(21)	8
$96 \times 48^3$	5.5	p	0.133830	0.09614(2)	2.454(178)	6.787(19)	4.867(12)	4
$192 \times 48^3$	5.7	o	0.136200	0.01691(2)	0.586(43)	11.48(24)	14.02(6)	4
$192 \times 48^3$	5.7	o	0.135570	0.03683(2)	1.277(94)	10.53(12)	11.87(7)	4
$192 \times 48^3$	5.7	o	0.134450	0.07209(2)	2.500(184)	9.50(5)	9.821(36)	8

**Table 4:** Overview of the ensembles generated with  $N_f = 2$   $\mathcal{O}(a)$  improved Wilson fermions. The columns show the lattice sizes, the gauge coupling  $\beta = 6/g_0^2$ , the boundary conditions (periodic (p) or open (o)), the hopping parameter  $\kappa$  (which is related to the bare mass  $m_0$  through  $\kappa = 1/(2am_0 + 8)$ ), the PCAC mass  $am$ , the ratio of the RGI mass  $M$  to the  $\Lambda$  parameter (computed using eq. (4.10)), the scales  $r_0/a$  and  $t_0/a^2$  and the total statistics in molecular dynamics units.

In table 6 we list the values of the hadronic scale  $L_1/a$  [21, 34]. At  $\beta = 5.3, 5.5$  they are taken from Table 7 of [21]. At the other  $\beta$  values they are obtained from a quadratic fit in  $\beta$  of  $\ln(L_1/a)$ , where data for the latter are taken from Table 13 of [21]. The lattice spacing for  $\beta > 5.5$  (not covered by the simulations in [21]) can be inferred from the value  $L_1 = 0.400(10)\text{fm}$  determined in [21].

### C.1 Mass corrections

The data for a hadronic scale  $m^{\text{had}}$  such as  $r_0^{-1}$ ,  $t_0^{-1/2}$  obtained from the simulations with standard Wilson fermions are corrected for small mismatches of the values  $M/\Lambda$  compared to the target values  $M_t/\Lambda$  given in eq. (4.1), see table 4. This is done by fitting the  $\beta = 5.7$  data to the form

$$am^{\text{had}}(M) = s_1 \times (M/\Lambda)^\alpha, \quad (\text{C.1})$$

with fit coefficients  $s_1$  and  $\alpha$ . This fit formula is motivated by eq. (3.12) taking the asymptotic expression  $P = (M/\Lambda_f)^{\eta_0}$ . For example for  $m^{\text{had}} = 1/\sqrt{t_0}$  we get  $\alpha = 0.123(2)$

$\frac{T}{a} \times (\frac{L}{a})^3$	$\beta$	$\kappa$	$a\mu$	$M/\Lambda$	$r_0/a$	$t_0/a^2$	kMDU
$120 \times 32^3$	5.300	0.136457	0.024505	0.5900	–	4.174(13)	4.3
$120 \times 32^3$	5.500	0.1367749	0.018334	0.5900	8.77(15)	7.917(82)	8
$192 \times 48^3$	5.700	0.136687	0.013713	0.5900	–	14.40(10)	5.8
$120 \times 32^3$	5.500	0.1367749	0.039776	1.2800	8.010(62)	6.871(33)	8
$192 \times 48^3$	5.700	0.136687	0.029751	1.2800	–	12.668(39)	16.2
$120 \times 32^3$	5.500	0.1367749	0.077687	2.5000	7.392(62)	5.836(27)	8
$192 \times 48^3$	5.700	0.136687	0.058108	2.5000	–	10.916(38)	9
$192 \times 48^3$	5.600	0.136710	0.130949	4.8700	–	6.561(12)	16
$120 \times 32^3$	5.700	0.136698	0.113200	4.8703	9.123(57)	9.104(36)	17.2
$192 \times 48^3$	5.880	0.136509	0.087626	4.8700	11.946(55)	15.622(62)	23.1
$192 \times 48^3$	6.000	0.136335	0.072557	4.8700	14.34(10)	22.39(12)	22.4
$192 \times 48^3$	5.600	0.136710	0.155367	5.7781	–	6.181(11)	2.1
$192 \times 48^3$	5.700	0.136687	0.1343	5.7781	–	8.565(31)	2.7
$120 \times 32^3$	5.880	0.136509	0.103965	5.7781	–	14.916(93)	59.9

**Table 5:** Overview of the ensembles generated with  $N_f = 2$  twisted mass fermions at maximal twist. The columns show the lattice sizes, the gauge coupling  $\beta = 6/g_0^2$ , the hopping parameter  $\kappa$  (for maximal twist), the twisted mass parameter  $a\mu$ , the ratio of the RGI mass  $M$  to the  $\Lambda$  parameter (computed using eq. (4.10)), the scales  $r_0/a$  (where it is measured) and  $t_0/a^2$  and the total statistics in molecular dynamics units.

and for  $m^{\text{had}} = 1/r_0$  we get  $\alpha = 0.139(12)$  which are close to  $\eta_0 = 0.121212$ . The corrected values  $m^{\text{had}}(M_t)$  are computed as

$$\ln(am^{\text{had}}(M_t)) = \ln(am^{\text{had}}(M)) + \alpha \ln(M_t/M). \quad (\text{C.2})$$

Note that eq. (C.2) being a small correction is applied for all lattice spacings  $a$ . Moreover the  $\Lambda$  parameter drops out in eq. (C.2). Since the main contribution to the error on  $M/\Lambda$  comes from  $\Lambda L_1$ , it does not affect the mass corrections. In order to determine the final error of  $am^{\text{had}}(M_t)$ , we propagate the error of the exponent  $\alpha$  and linearly add its contribution (for a conservative estimate) multiplied by a factor of two.

No corrections is needed for the hadronic scales from twisted mass simulations since their parameters are tuned for the target mass values, see section 4.2.3.

## References

- [1] M. Lüscher, *Properties and uses of the Wilson flow in lattice QCD*, *JHEP* **08** (2010) 071 [[1006.4518](#)].
- [2] S. Weinberg, *Effective gauge theories*, *Phys.Lett.* **B91** (1980) 51.
- [3] W. Bernreuther and W. Wetzel, *Decoupling of Heavy Quarks in the Minimal Subtraction Scheme*, *Nucl.Phys.* **B197** (1982) 228.
- [4] K. Chetyrkin, J. H. Kühn and C. Sturm, *QCD decoupling at four loops*, *Nucl.Phys.* **B744** (2006) 121 [[hep-ph/0512060](#)].

$\beta$	$L_1/a$	$a$ [fm]
5.30	6.195(51)	0.066
5.50	8.280(80)	0.049
5.60	9.569(99)	$\approx 0.042$
5.70	11.07(17)	$\approx 0.036$
5.88	14.30(24)	$\approx 0.028$
6.00	17.27(70)	$\approx 0.023$

**Table 6:** The values of the scale  $L_1/a$  used in our simulations and the corresponding lattice spacings.

- [5] Y. Schröder and M. Steinhauser, *Four-loop decoupling relations for the strong coupling*, *JHEP* **01** (2006) 051 [[hep-ph/0512058](#)].
- [6] T. van Ritbergen, J. A. M. Vermaseren and S. A. Larin, *The Four loop beta function in quantum chromodynamics*, *Phys. Lett.* **B400** (1997) 379 [[hep-ph/9701390](#)].
- [7] M. Czakon, *The Four-loop QCD beta-function and anomalous dimensions*, *Nucl. Phys.* **B710** (2005) 485 [[hep-ph/0411261](#)].
- [8] P. A. Baikov, K. G. Chetyrkin and J. H. Kühn, *Five-Loop Running of the QCD coupling constant*, *Phys. Rev. Lett.* **118** (2017) 082002 [[1606.08659](#)].
- [9] T. Luthe, A. Maier, P. Marquard and Y. Schröder, *Towards the five-loop Beta function for a general gauge group*, *JHEP* **07** (2016) 127 [[1606.08662](#)].
- [10] F. Herzog, B. Ruijl, T. Ueda, J. A. M. Vermaseren and A. Vogt, *The five-loop beta function of Yang-Mills theory with fermions*, *JHEP* **02** (2017) 090 [[1701.01404](#)].
- [11] ALPHA collaboration, M. Bruno, J. Finkenrath, F. Knechtli, B. Leder and R. Sommer, *Effects of Heavy Sea Quarks at Low Energies*, *Phys. Rev. Lett.* **114** (2015) 102001 [[1410.8374](#)].
- [12] S. Sint, *Lattice QCD with a chiral twist*, In *Perspectives in Lattice QCD, World Scientific 2008* (2007) [[hep-lat/0702008](#)].
- [13] R. Sommer, *A new way to set the energy scale in lattice gauge theories and its applications to the static force and  $\alpha_s$  in  $SU(2)$  Yang-Mills theory*, *Nucl. Phys.* **B411** (1994) 839 [[hep-lat/9310022](#)].
- [14] S. Borsanyi, S. Dür, Z. Fodor, C. Hoelbling, S. D. Katz et al., *High-precision scale setting in lattice QCD*, *JHEP* **1209** (2012) 010 [[1203.4469](#)].
- [15] R. Sommer, *Scale setting in lattice QCD*, *PoS LATTICE2013* (2014) 015 [[1401.3270](#)].
- [16] M. Bruno and R. Sommer, *On the  $N_f$ -dependence of gluonic observables*, *PoS (LATTICE2013)* 321 [[1311.5585](#)].



- [17] A. Kryjevski, *Heavy quark anti- $q$   $q$  matrix elements in the nucleon from perturbative QCD*, *Phys. Rev.* **D70** (2004) 094028 [[hep-ph/0312196](#)].
- [18] A. G. Grozin, M. Hoeschele, J. Hoff and M. Steinhauser, *Simultaneous decoupling of bottom and charm quarks*, *JHEP* **1109** (2011) 066 [[1107.5970](#)].
- [19] R. Sommer, *Introduction to Non-perturbative Heavy Quark Effective Theory*, in *Modern perspectives in lattice QCD: Quantum field theory and high performance computing. Proceedings, International School, 93rd Session, Les Houches, France, August 3-28, 2009*, pp. 517–590, 2010, [1008.0710](#).
- [20] PARTICLE DATA GROUP collaboration, C. Patrignani et al., *Review of Particle Physics*, *Chin. Phys.* **C40** (2016) 100001.
- [21] P. Fritzsche, F. Knechtli, B. Leder, M. Marinkovic, S. Schaefer et al., *The strange quark mass and Lambda parameter of two flavor QCD*, *Nucl.Phys.* **B865** (2012) 397 [[1205.5380](#)].
- [22] J. Heitger, G. M. von Hippel, S. Schaefer and F. Virotta, *Charm quark mass and D-meson decay constants from two-flavour lattice QCD*, *PoS LATTICE2013* (2014) 475 [[1312.7693](#)].
- [23] C. W. Bernard, T. Burch, K. Orginos, D. Toussaint, T. A. DeGrand et al., *The Static quark potential in three flavor QCD*, *Phys.Rev.* **D62** (2000) 034503 [[hep-lat/0002028](#)].
- [24] R. Narayanan and H. Neuberger, *Infinite  $N$  phase transitions in continuum Wilson loop operators*, *JHEP* **03** (2006) 064 [[hep-th/0601210](#)].
- [25] M. Lüscher and P. Weisz, *Perturbative analysis of the gradient flow in non-abelian gauge theories*, *JHEP* **1102** (2011) 051 [[1101.0963](#)].
- [26] K. G. Wilson, *Confinement of quarks*, *Phys. Rev.* **D10** (1974) 2445.
- [27] B. Sheikholeslami and R. Wohlert, *Improved Continuum Limit Lattice Action for QCD with Wilson Fermions*, *Nucl. Phys.* **B259** (1985) 572.
- [28] M. Lüscher, S. Sint, R. Sommer and P. Weisz, *Chiral symmetry and  $O(a)$  improvement in lattice QCD*, *Nucl. Phys.* **B478** (1996) 365 [[hep-lat/9605038](#)].
- [29] ALPHA collaboration, R. Frezzotti, P. A. Grassi, S. Sint and P. Weisz, *Lattice QCD with a chirally twisted mass term*, *JHEP* **08** (2001) 058 [[hep-lat/0101001](#)].
- [30] ALPHA collaboration, K. Jansen and R. Sommer,  *$O(a)$  improvement of lattice QCD with two flavors of Wilson quarks*, *Nucl. Phys.* **B530** (1998) 185 [[hep-lat/9803017](#)].
- [31] R. Frezzotti and G. C. Rossi, *Chirally improving Wilson fermions. 1.  $O(a)$  improvement*, *JHEP* **08** (2004) 007 [[hep-lat/0306014](#)].
- [32] P. Dimopoulos, H. Simma and A. Vladikas, *Quenched  $B(K)$ -parameter from Osterwalder-Seiler  $tmQCD$  quarks and mass-splitting discretization effects*, *JHEP* **07** (2009) 007 [[0902.1074](#)].



- [33] ALPHA collaboration, F. Knechtli, T. Korzec, B. Leder and G. Moir, *Power corrections from decoupling of the charm quark*, *Phys. Lett.* **B774** (2017) 649 [[1706.04982](#)].
- [34] ALPHA collaboration, B. Blossier, M. Della Morte, P. Fritzsch, N. Garron, J. Heitger, H. Simma et al., *Parameters of Heavy Quark Effective Theory from  $N_f=2$  lattice QCD*, *JHEP* **09** (2012) 132 [[1203.6516](#)].
- [35] S. Sint and R. Sommer, *The running coupling from the QCD Schrödinger functional: A one loop analysis*, *Nucl. Phys.* **B465** (1996) 71 [[hep-lat/9508012](#)].
- [36] M. Lüscher, S. Sint, R. Sommer and P. Weisz, *Chiral symmetry and  $O(a)$  improvement in lattice QCD*, *Nucl. Phys.* **B478** (1996) 365 [[hep-lat/9605038](#)].
- [37] M. Della Morte, R. Sommer and S. Takeda, *On cutoff effects in lattice QCD from short to long distances*, *Phys.Lett.* **B672** (2009) 407 [[0807.1120](#)].
- [38] M. Dalla Brida, T. Korzec, S. Sint and P. Vilaseca, *High precision renormalization of the flavour non-singlet Noether currents in lattice QCD with Wilson quarks*, [1808.09236](#).
- [39] ALPHA collaboration, M. Della Morte et al., *Non-perturbative quark mass renormalization in two-flavor QCD*, *Nucl. Phys.* **B729** (2005) 117 [[hep-lat/0507035](#)].
- [40] ALPHA collaboration, M. Della Morte et al., *Computation of the strong coupling in QCD with two dynamical flavours*, *Nucl. Phys.* **B713** (2005) 378 [[hep-lat/0411025](#)].
- [41] M. Della Morte, A. Shindler and R. Sommer, *On lattice actions for static quarks*, *JHEP* **08** (2005) 051 [[hep-lat/0506008](#)].
- [42] M. Donnellan, F. Knechtli, B. Leder and R. Sommer, *Determination of the Static Potential with Dynamical Fermions*, *Nucl.Phys.* **B849** (2011) 45 [[1012.3037](#)].
- [43] A. Hasenfratz and F. Knechtli, *Flavor symmetry and the static potential with hypercubic blocking*, *Phys. Rev.* **D64** (2001) 034504 [[hep-lat/0103029](#)].
- [44] ETM collaboration, K. Jansen, C. Michael and C. Urbach, *The eta-prime meson from lattice QCD*, *Eur. Phys. J.* **C58** (2008) 261 [[0804.3871](#)].
- [45] S. Bernardson, P. McCarty and C. Thron, *Monte Carlo methods for estimating linear combinations of inverse matrix entries in lattice QCD*, *Comput. Phys. Commun.* **78** (1993) 256.
- [46] M. Marinkovic and S. Schaefer, *Comparison of the mass preconditioned HMC and the DD-HMC algorithm for two-flavour QCD*, *PoS LATTICE2010* (2010) 031 [[1011.0911](#)].
- [47] ALPHA collaboration, S. Schaefer, R. Sommer and F. Virotta, *Critical slowing down and error analysis in lattice QCD simulations*, *Nucl.Phys.* **B845** (2011) 93 [[1009.5228](#)].

- [48] ALPHA collaboration, M. Bruno, S. Schaefer and R. Sommer, *Topological susceptibility and the sampling of field space in  $N_f = 2$  lattice QCD simulations*, *JHEP* **1408** (2014) 150 [[1406.5363](#)].
- [49] M. Lüscher and S. Schaefer, *Lattice QCD with open boundary conditions and twisted-mass reweighting*, *Comput.Phys.Commun.* **184** (2013) 519 [[1206.2809](#)].
- [50] M. Hasenbusch, *Speeding up the hybrid Monte Carlo algorithm for dynamical fermions*, *Phys. Lett.* **B519** (2001) 177 [[hep-lat/0107019](#)].
- [51] M. Lüscher, *Solution of the Dirac equation in lattice QCD using a domain decomposition method*, *Comput. Phys. Commun.* **156** (2004) 209 [[hep-lat/0310048](#)].
- [52] A. Frommer, K. Kahl, S. Krieg, B. Leder and M. Rottmann, *Adaptive Aggregation Based Domain Decomposition Multigrid for the Lattice Wilson Dirac Operator*, *SIAM J. Sci. Comput.* **36** (2014) A1581 [[1303.1377](#)].
- [53] C. Alexandrou, S. Bacchio, J. Finkenrath, A. Frommer, K. Kahl and M. Rottmann, *Adaptive Aggregation-based Domain Decomposition Multigrid for Twisted Mass Fermions*, *Phys. Rev.* **D94** (2016) 114509 [[1610.02370](#)].
- [54] H. Panagopoulos and Y. Proestos, *The Critical hopping parameter in  $O(a)$  improved lattice QCD*, *Phys. Rev.* **D65** (2002) 014511 [[hep-lat/0108021](#)].
- [55] ALPHA collaboration, U. Wolff, *Monte Carlo errors with less errors*, *Comput. Phys. Commun.* **156** (2004) 143 [[hep-lat/0306017](#)].
- [56] ALPHA collaboration, F. Knechtli, M. Bruno, J. Finkenrath, B. Leder and R. Sommer, *Perturbative versus non-perturbative decoupling of heavy quarks*, *PoS LATTICE2015* (2016) 256 [[1511.04914](#)].
- [57] ALPHA collaboration, S. Capitani, M. Lüscher, R. Sommer and H. Wittig, *Non-perturbative quark mass renormalization in quenched lattice QCD*, *Nucl. Phys.* **B544** (1999) 669 [[hep-lat/9810063](#)].
- [58] O. Bär and M. Golterman, *Chiral perturbation theory for gradient flow observables*, *Phys.Rev.* **D89** (2014) 034505 [[1312.4999](#)].
- [59] J. Hisano, *Effective theory approach to direct detection of dark matter*, [1712.02947](#).
- [60] L. Vecchi, *WIMPs and Un-Naturalness*, [1312.5695](#).
- [61] J. Ellis, N. Nagata and K. A. Olive, *Uncertainties in WIMP Dark Matter Scattering Revisited*, *Eur. Phys. J.* **C78** (2018) 569 [[1805.09795](#)].
- [62] S. Aoki et al., *Review of lattice results concerning low-energy particle physics*, *Eur. Phys. J.* **C77** (2017) 112 [[1607.00299](#)].
- [63] ALPHA collaboration, M. Bruno, M. Dalla Brida, P. Fritzsch, T. Korzec, A. Ramos, S. Schaefer et al., *QCD Coupling from a Nonperturbative Determination of the Three-Flavor  $\Lambda$  Parameter*, *Phys. Rev. Lett.* **119** (2017) 102001 [[1706.03821](#)].

- [64] B. A. Kniehl, A. V. Kotikov, A. I. Onishchenko and O. L. Veretin, *Strong-coupling constant with flavor thresholds at five loops in the anti- $\overline{MS}$  scheme*, *Phys. Rev. Lett.* **97** (2006) 042001 [[hep-ph/0607202](#)].
- [65] K. G. Chetyrkin, *Quark mass anomalous dimension to  $O(\alpha_s^4)$* , *Phys. Lett.* **B404** (1997) 161 [[hep-ph/9703278](#)].
- [66] J. A. M. Vermaseren, S. A. Larin and T. van Ritbergen, *The four loop quark mass anomalous dimension and the invariant quark mass*, *Phys. Lett.* **B405** (1997) 327 [[hep-ph/9703284](#)].